

LONG-TERM VARIABILITY OF H₂CO MASERS IN STAR-FORMING REGIONS

N. ANDREEV,¹ E. D. ARAYA,¹ I. M. HOFFMAN,² P. HOFNER,^{3,*} S. KURTZ,⁴ H. LINZ,⁵ L. OLMÍ,^{6,7} AND I. LORRAN-COSTA¹

¹*Physics Department, Western Illinois University, 1 University Circle, Macomb, IL 61455, USA.*

²*Quest University, 3200 University Boulevard, Squamish, British Columbia V8B0N8, Canada.*

³*New Mexico Institute of Mining and Technology, Physics Department, 801 Leroy Place, Socorro, NM 87801, USA.*

⁴*Instituto de Radioastronomía y Astrofísica, Universidad Nacional Autónoma de México, Apdo. Postal 3-72, 58090, Morelia, Michoacán, Mexico.*

⁵*Max-Planck-Institut für Astronomie, Königstuhl 17, D-69117, Heidelberg, Germany.*

⁶*INAF, Osservatorio Astrofisico di Arcetri, Largo E. Fermi 5, I-50125, Firenze, Italy.*

⁷*University of Puerto Rico, Río Piedras Campus, Physics Dept., Box 23343, UPR Station, San Juan, PR 00931, USA.*

(Received September 4, 2017; Revised September 4, 2017; Accepted September 7, 2017)

Submitted to ApJS

ABSTRACT

We present results of a multi-epoch monitoring program on variability of 6 cm formaldehyde (H₂CO) masers in the massive star forming region NGC 7538 IRS 1 from 2008 to 2015 conducted with the GBT, WSRT, and VLA. We found that the similar variability behaviors of the two formaldehyde maser velocity components in NGC 7538 IRS 1 (which was pointed out by Araya and collaborators in 2007) have continued. The possibility that the variability is caused by changes in the maser amplification path in regions with similar morphology and kinematics is discussed. We also observed 12.2 GHz methanol and 22.2 GHz water masers toward NGC 7538 IRS 1. The brightest maser components of CH₃OH and H₂O species show a decrease in flux density as a function of time. The brightest H₂CO maser component also shows a decrease in flux density and has a similar LSR velocity to the brightest H₂O and 12.2 GHz CH₃OH masers. The line parameters of radio recombination lines and the 20.17 and 20.97 GHz CH₃OH transitions in NGC 7538 IRS 1 are also reported. In addition, we observed five other 6 cm formaldehyde maser regions. We found no evidence of significant variability of the 6 cm masers in these regions with respect to previous observations, the only possible exception being the maser in G29.96–0.02. All six sources were also observed in the H₂¹³CO isotopologue transition of the 6 cm H₂CO line; H₂¹³CO absorption was detected in five of the sources. Estimated column density ratios [H₂¹²CO]/[H₂¹³CO] are reported.

Keywords: radio lines: ISM — Masers — ISM: HII regions, molecules, individual objects (NGC 7538 IRS 1, G23.01–0.41, G23.71–0.20, G25.83–0.18, G29.96–0.02, IRAS 18566+0408)

Corresponding author: E. D. Araya
ed-araya@wiu.edu

* Adjunct Astronomer at the National Radio Astronomy Observatory, 1003 Lopezville Road, Socorro, NM 87801, USA.

1. INTRODUCTION

Since their discovery in 1965 (Weaver et al. 1965), astrophysical masers have been the object of active research. They have been detected in different regions, including clouds of water vapor around moons of Saturn (Pogrebenko et al. 2009), atmospheres of comets (Biraud et al. 1974; Turner 1974; Bockelee-Morvan et al. 1994), circumstellar envelopes of evolved stars (e.g., Wilson & Barrett 1968), supernova remnants (e.g., Frail et al. 1994), and star forming regions (e.g., Robinson & McGee 1967). In addition, masers and megamasers have been found in extragalactic environments (e.g., Baan 1985; Haschick et al. 1994; Lo 2005; Sjouwerman et al. 2010). There are several types of masers which have been detected exclusively in high-mass star forming regions (HMSFR) including 6.7 and 12.2 GHz methanol and 6 cm (4.83 GHz) formaldehyde masers (e.g., Walsh et al. 1998; Breen et al. 2013; Araya et al. 2007a; Araya et al. 2015). These masers are not only signposts of high-mass star formation but also help trace small-scale dynamics, morphology, and the locations of outflows and accretion disks (e.g., Bartkiewicz et al. 2009; Sanna et al. 2010; Goddi et al. 2011; Torrelles et al. 2011; Moscadelli et al. 2011).

Astrophysical masers exhibit diverse temporal variability with time scales ranging from less than a day to years, from aperiodic flares to quasi-periodic and sinusoidal patterns (e.g., Felli et al. 2007; Goedhart et al. 2004; Goedhart et al. 2012; Goedhart et al. 2014). Excluding stellar masers (i.e., associated with evolved stars), maser variability is not yet well understood. In some cases, flux density variability of certain maser species (6.7 and 12.2 GHz methanol, 6 cm formaldehyde, 6.035 GHz hydroxyl, and 22.2 GHz water masers) in HMSFR is predictable, such as monotonic increase/decrease in flux density and periodic maser flares (e.g., Goedhart et al. 2003; Araya et al. 2010; Al-Marzouk et al. 2012; Maswanganye et al. 2016). A particularly interesting recent example is the anti-correlated flares of methanol and water masers in the intermediate-mass young stellar object G107.298+5.639, which could be tracing periodic accretion instabilities in a protobinary disk (Szymczak et al. 2016). The study of correlated variability of different maser species and velocity components of a single maser transition is aimed to investigate the mechanism of maser excitation and to use masers as astrophysical probes to better understand the processes of intermediate and high-mass star formation.

The 6 cm line of formaldehyde (H_2CO) is a rare maser transition that has been reported toward nine HMSFRs in our Galaxy: NGC 7538 IRS 1 (Downes & Wilson 1974; Hoffman et al. 2003), Sgr B2 (Whiteoak & Gardner 1983; Mehringer et al. 1994; Hoffman et al. 2007), G29.96–0.02 (Pratap et al. 1994; Hoffman et al. 2003), IRAS 18566+0408 (G37.55+0.20; Araya et al. 2004b), G23.71–0.20 (Araya et al. 2006), G23.01–0.41 (Araya et al. 2008), G25.83–0.18 (Araya et al. 2008), G32.74–0.07 (Araya et al. 2015), and G0.38+0.04 (Ginsburg et al. 2015), and three extragalactic regions (Baan et al. 1986; Araya et al. 2004a; see however Mangum et al. 2008).

The first 6 cm formaldehyde maser was detected in NGC 7538 IRS 1 (Downes & Wilson 1974; Rots et al. 1981). This region is located at a distance of $2.65^{+0.12}_{-0.11}$ kpc (Moscadelli et al. 2009) and it is one of the richest maser sites known (e.g., Galván-Madrid et al. 2010; Surcis et al. 2011; Hoffman & Kim 2011). Interferometric observations of the double-peaked 6 cm formaldehyde maser in NGC 7538 IRS 1 show that the two velocity components originate from two regions oriented approximately NE-SW (Figure 1), which are separated by ~ 200 AU in the plane of the sky (based on Hoffman et al. 2003 and the distance reported by Moscadelli et al. 2009). VLBA observations by Hoffman et al. (2003) show that the NE maser (Component I) has a velocity gradient of 1 km s^{-1} over a projected scale of ~ 100 AU. The formaldehyde masers could be located inside of (or close to) a possible circumbinary envelope that has been proposed by Goddi et al. (2015). While the H_2CO maser Component II seems to reside approximately between two 6.7 GHz methanol maser clusters (A and C, Figure 1; see also Moscadelli & Goddi 2014), Component I is very close (in projection) to the northern 6.7 GHz maser cluster A, which shows small-scale velocity gradients in thermal molecular lines from NH_3 and CH_3OH (Beuther et al. 2017).

The two formaldehyde masers did not show significant variability over a period of about eight years after their discovery. After 1982, the intensity of Component I increased while Component II showed no variability; approximately 14 years later, the intensity of Component II started to increase. After the onset of variability, both components showed similar variability slopes, which suggested a connection between the flux density changes of the maser regions (Araya et al. 2007b).

In this paper we report monitoring observations of the 6 cm formaldehyde masers in NGC 7538 IRS 1 to investigate whether the similar variability trend of both components has continued. We also investigate variability of 6 cm formaldehyde masers in five other star forming regions. We report detection of absorption of 4.59 GHz H_2^{13}CO in five

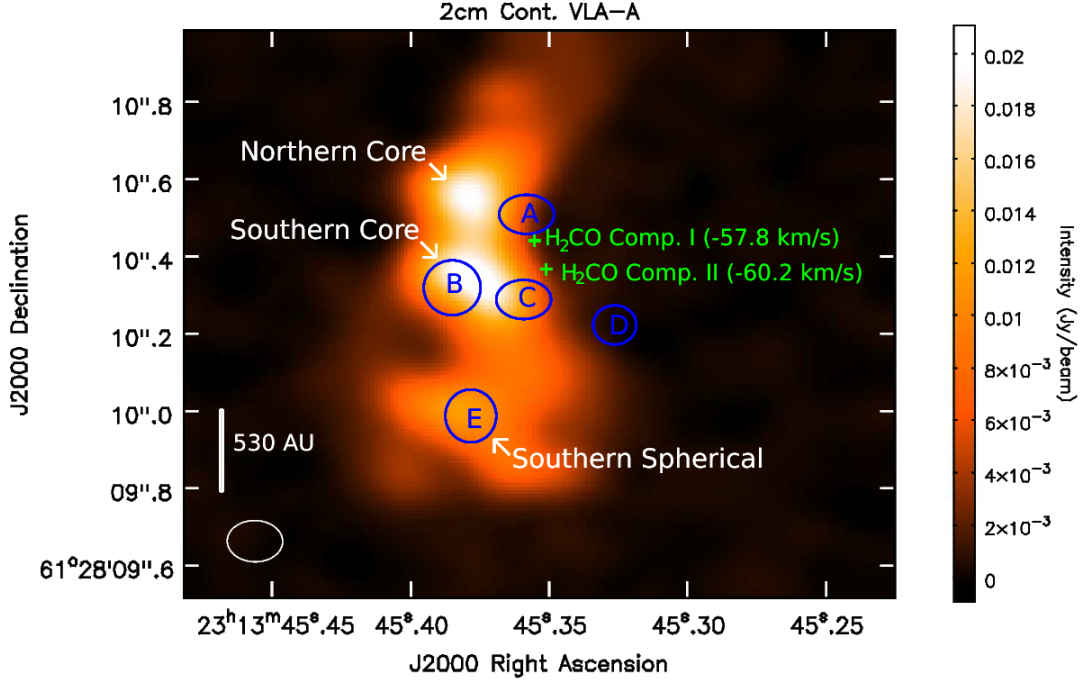


Figure 1. NGC 7538 IRS 1 region; 2 cm radio continuum is shown in colors (VLA A-configuration, 2 cm Ku-band observations, VLA archive, project AM0169). The crosses show the location of the 6 cm H₂CO masers (Hoffman et al. 2003). The blue ellipses show the approximate location of 6.7 GHz CH₃OH maser groups. The identification of the CH₃OH maser groups (A to E) and the radio continuum sources (Northern Core, Southern Core, and Southern Spherical) are as presented by Moscadelli & Goddi (2014).

of the six HMSFRs in our sample, as well as observations of 12.2 GHz methanol masers, 22.2 GHz water masers, and 20.17 and 20.97 GHz methanol absorption lines in NGC 7538 IRS 1.¹

2. OBSERVATIONS

2.1. Robert C. Byrd Green Bank Telescope Observations

We used the Robert C. Byrd Green Bank Telescope (GBT, Green Bank Observatory) in West Virginia in our monitoring program to study the long term variability of formaldehyde masers in NGC 7538 IRS 1. The pointing position of all observations was R.A. = $23^h 13^m 45.36^s$, Decl. = $+61^\circ 28' 10.5''$ (J2000; Galván-Madrid et al. 2010). Doppler tracking was centered at a LSR velocity of -55.00 km s^{-1} . All data reduction was done using GBTIDL routines provided by NRAO. We report GBT observations from May 2008 to May 2011 of NGC 7538 IRS 1 in the C (6 cm), Ku (2 cm), and K (1.3 cm) bands. We used the GBT spectrometer with 4 spectral windows (see Table 1). After calibration, orthogonal polarization spectra were checked for consistency and averaged. A linear baseline was subtracted. Some spectra were smoothed to improve signal-to-noise; the final channel separations after smoothing are listed in Table 1.

2.1.1. C-Band Observations

The GBT half-power beam width (HPBW) within the frequency range of our C-Band observations (4.3 to 5.0 GHz) is between $2.9'$ and $2.5'$. We conducted six epochs of C-Band observations (see Table 1) of NGC 7538 IRS 1: one in frequency switching mode and five in position switching mode. In addition, two observations of IRAS 18566+0408

¹ This work is based on Chapter 3 of the MS Thesis “From Diffuse Clouds to Massive Star Forming Regions” by N. Andreev, WIU, 2014.

Table 1. Spectral Lines

Molecule	Transition*	Rest Frequency* (GHz)	Epoch/Mode ⁺	Chan. Spacing (km s ⁻¹)	RRLs in Bandpass
H ₂ C ¹⁸ O	1(1,0)-1(1,1)	4.3887970	1a, 2c, 3c, 4ac, 5c, 6c	0.42	
H ₂ ¹³ CO	1(1,0)-1(1,1)	4.5930885	1a, 2c, 3c, 4ac, 5c, 6c	0.40 ¹	H141 β
H ₂ CO	1(1,0)-1(1,1)	4.8296594	1a, 2c, 3c, 4ac, 5c, 6c	0.095/0.57 ¹	H174 δ ²
			7w, 8w	0.095	
			9v	0.061	
CH ₃ OH	3(1,2)-3(1,3) A ⁻⁺	5.0053208	1a, 2c, 3c, 4ac, 5c, 6c	0.37	H137 β , H109
CH ₃ OH	2(0,2)-3(-1,3) E	12.1785970	1b, 5b	0.075	
H ₂ ¹³ CO	2(1,1)-2(1,2)	13.7788041	1b, 5b	0.27	
H ₂ CO	2(1,1)-2(1,2)	14.4884801	1b, 5b	0.32	
¹³ CH ₃ OH	2(0,2)-3(-1,3) E	14.7822120	1b, 5b	0.25	
CH ₃ OH	2(1,1)-3(0,3) E	19.9673961	1b, 2b, 5b	0.18	H86 β ³
CH ₃ OH	11(1,11)-10(2,8) A ⁺⁺	20.1710890	1b, 2b, 5b	0.18	
CH ₃ OH	10(1,10)-11(2,9) A ⁺⁺ $\nu_t=1$	20.9706510	1b, 2b, 5b	0.35	
H ₂ O	6(1,6)-5(2,3)	22.2350800	1b, 2b, 5b	0.16	

*Quantum numbers and rest frequencies obtained from the Cologne Database for Molecular Spectroscopy (Müller et al. 2005), the Lovas database (<http://www.nist.gov/pml/data/micro/index.cfm>), and the JPL Molecular Spectroscopy catalog (Pickett et al. 1998) accessed through *splatalogue* (<http://www.cv.nrao.edu/php/splat/>).

⁺ Observing epochs: 1. 2008-May-05; 2. 2009-May-18; 3. 2009-July-03; 4. 2009-July-17; 5. 2010-May-07; 6. 2011-May-31; 7. 2014-December-07, 8. 2015-May-29, 9. 2015-June-28. Observing Modes: a. GBT observations, frequency switching; b. GBT observations, beam switching; c. GBT observations, position switching; w. WSRT observations, v. VLA observations.

¹ Channel width of RRLs. The isotopologue spectra were smoothed to different channel widths: 0.8 km s⁻¹ (G23.01–0.41, G23.71–0.20, IRAS 18566+0408), 1.2 km s⁻¹ (NGC 7538 IRS 1), and 1.6 km s⁻¹ (G25.83–0.18, G29.96–0.02).

² The H174 δ was only observed in ‘c’ mode (GBT observations, position switching).

³ The H86 β line was only observed in Epoch 1 because a bandwidth of 50 MHz was used in the K-Band observations. The line was outside the bandpass in the other epochs (2 and 5) because of a smaller bandwidth (12.5 MHz).

and a single observation of G23.01–0.41, G23.71–0.20, G25.83–0.18, and G29.96–0.02 were conducted (Table 2). Specifically:

- Epoch 1: The C-Band observations of NGC 7538 IRS 1 and IRAS 18566+0408 were done in frequency switching mode (± 3.125 MHz switching cycle), 12.5 MHz (~ 300 km s⁻¹) bandwidth, 9 level sampling, 8192 channels (1.526 kHz, 0.095 km s⁻¹ channel width), dual linear polarization.
- Epochs 2 - 6: The C-Band observations of NGC 7538 IRS 1 were done in position switching mode to improve the baseline quality with respect to frequency switching observations. We used 12.5 MHz bandwidth, 4096 channels (3.052 kHz, ~ 0.19 km s⁻¹ initial channel separation), and dual linear polarization.
- Epoch 4: The C-Band observations of G23.01–0.41, G23.71–0.20, G25.83–0.18, G29.96–0.02, and IRAS 18566+0408 were done in frequency switching mode (± 3.125 MHz switching cycle), 12.5 MHz bandwidth, 9 level sampling, 8192 channels (1.526 kHz), dual linear polarization.

Table 2. Observed Sources

Name	<i>RA</i> (<i>J</i> 2000)	<i>Decl.</i> (<i>J</i> 2000)	Epoch/Mode ⁺	Adopted Distance	Ref. Distance
	(h m s)	(° ' ")		(kpc)	
G23.01–0.41	18 34 40.3	–09 00 38	4a	4.59 ^{+0.38} _{–0.33}	1
G23.71–0.20	18 35 12.4	–08 17 39	4a	6.21 ^{+1.0} _{–0.80}	2
G25.83–0.18	18 39 03.6	–06 24 11	4a	5.0 ^{+0.3} _{–0.3}	3
G29.96–0.02	18 46 03.8	–02 39 22	4a	5.3 ^{+0.5} _{–0.5}	4
IRAS 18566+0408	18 59 10.0	+04 12 15	1a and 4a	6.7 ^{+1.4} _{–1.4}	5
NGC 7538 IRS 1	23 13 45.36	+61 28 10.5	1ab, 2bc, 3c, 4c, 5bc, 6c, 7w, 8w, 9v	2.65 ^{+0.12} _{–0.11}	6

⁺ Same notation as in Table 1.

NOTE— Reference of adopted distance: (1) [Brunthaler et al. \(2009\)](#); (2) [Sanna et al. \(2014a\)](#); (3) [Green & McClure-Griffiths \(2011\)](#); (4) [Reid et al. \(2014\)](#); (5) [Araya et al. \(2004b\)](#); (6) [Moscadelli et al. \(2009\)](#).

For NGC 7538 IRS 1 the total integration times on-source were 5 minutes for epochs 1 and 5; 10 minutes for epochs 2 and 4; 18 minutes for epoch 3; and approximately 3 minutes for epoch 6. For G25.83–0.18 and G29.96–0.02 the integration time per source was about 14 minutes; for G23.01–0.41, G23.71–0.20, and IRAS 18566+0408 was about 28 minutes each during epoch 4. The integration time on IRAS 18566+0408 in epoch 1 was approximately 9 minutes. To derive pointing and focus corrections we observed the GBT calibrators: J2148+6107 in epochs 1, 2, 3, 5, and 6; 3C48 in epochs 1, 2, 4, 5, and 6; and J1851+0035 in epochs 1 and 4. The pointing corrections were smaller than 4". The system temperature for the six epochs of observations was approximately 23 K. We measured a continuum flux density of 5.95 Jy at 6 cm for 3C48 in epoch 5, which agrees within 9% with the expected value of 5.45 Jy ([Perley and Butler 2013](#)). The percentage error is less than 9% for all other epochs.

2.1.2. Ku-Band Observations

The HPBW of the GBT is between 60" and 51" at 12.2 to 14.8 GHz. The Ku-Band observations were done in beam switching (nod) mode; the two beams are separated by 330". We conducted observations in epochs 1 and 5 (see Table 1).

- Epoch 1: The total integration time on-source was 8 min. The system temperature was approximately 30 K. We obtained pointing and focus corrections from observations of J2148+6107; the pointing corrections were smaller than 4". We applied atmospheric opacity corrections (at zenith) between 0.011 and 0.014 Nepers within the 12.1 to 14.8 GHz frequency range, which were determined based on data from nearby weather stations accessed through the GBT software CLEO. We also observed the quasar 3C48 to estimate the flux density calibration uncertainty of our observations. We measured $S_\nu = 1.79$ Jy at 14.488 GHz, which agrees within 5% with the expected value of 1.88 Jy ([Perley and Butler 2013](#)).
- Epoch 5: The total on-source integration time was 4 minutes. The system temperature was approximately 27 K. We applied atmospheric opacity corrections (at zenith) between 0.018 and 0.025 Nepers within the 12.1 to 14.8 GHz frequency range.

2.1.3. K-Band Observations

The K-Band observations were conducted in beam switching mode (feed separation $\sim 3'$), dual circular polarization. The GBT HPBW between 19.9 and 22.2 GHz is between 38" and 34". We conducted observations in epochs 1, 2, and 5 (Table 1). The total integration times on-source were 15, 4, and 6 minutes, respectively. The system temperature varied between 24 and 50 K. We observed the quasars J2148+6107, 3C48, and 3C295 to derive pointing and focus corrections. The pointing corrections were smaller than 6".

- Epoch 1: we observed 3C295 to check the flux density calibration. We measured a continuum flux density of 1.01 Jy at 22.2 GHz, which agrees within 4% with the expected value of 0.97 Jy (Perley and Butler 2013). The atmospheric opacities at zenith were between 0.037 and 0.071 Nepers (19.9 to 22.2 GHz).
- Epoch 2: we observed two calibrators (3C48 and J2148+6107). We measured a continuum flux density of 1.35 Jy at 22.2 GHz for 3C48, which agrees within 7% with the expected value of 1.26 Jy (Perley and Butler 2013). The atmospheric opacities at zenith were between 0.023 and 0.039 Nepers (19.9 to 22.2 GHz).
- Epoch 5: The atmospheric opacities at zenith were between 0.042 and 0.093 Nepers (19.9 to 22.2 GHz).

2.2. Westerbork Synthesis Radio Telescope Observations

We observed the 6 cm H_2CO maser in NGC 7538 IRS 1 using the Westerbork Synthesis Radio Telescope² at epochs 7 and 8: 2014 December 07 and 2015 May 29. Only a subset of the array was available for the observations — eight antennas for the first epoch and six antennas for the second — with baseline lengths in the range 50–2550 m corresponding to a maximum angular sensitivity of $230''$. For both epochs the maser target was observed for 1.0 hr preceded and followed by observations of 3C48. The data were reduced using AIPS of the NRAO. For both epochs, 3C48 was observed to have a flux density of 5.1 Jy which is 6% below the expected value of 5.45 Jy (Perley and Butler 2013). Aside from initial amplitude and phase calibrations using 3C48, no self-calibration was applied. The spectra were formed as 1024 channels across a 312.5 kHz band for a velocity spacing of 19 m s^{-1} . The images from the two epochs have beams of approximately $60'' \times 3''$ at position angles of 30 and 10 degrees, respectively. The noise level in a single-channel image is $140 \text{ mJy beam}^{-1}$, consistent with instrumental expectations.

2.3. Karl G. Jansky Very Large Array Observations

The 6 cm H_2CO maser was also observed with the NRAO Karl G. Jansky Very Large Array (VLA) on June 28, 2015 (epoch 9) in A-configuration (synthesized beam: $0.89'' \times 0.33''$, -65° P.A.; $8.9''$ largest recoverable angular scale). The 6 cm H_2CO line ($\nu_0 = 4829.6594 \text{ MHz}$, see Table 1) was observed with 4096 channels, 4 MHz (248 km s^{-1}) bandwidth, and a channel width of 0.977 kHz (0.06 km s^{-1}). We used 3C286 (J1331+305) as flux density and bandpass calibrator and J2230+6946 as complex gain calibrator, which was observed for approximately 3 min before and after NGC 7538 IRS 1. The time on NGC 7538 IRS 1 was $\approx 13 \text{ min}$. All data reduction was done using the NRAO data reduction package CASA following standard spectral line data reduction procedures. Assuming a flux density of 7.365 Jy for 3C286 (Perley and Butler 2013) we measure a flux density of $1.00 \pm 0.01 \text{ Jy}$ for J2230+6946 using the CASA task `fluxscale`, which agrees within 10% with the value of 1.10 Jy at C-band listed in the VLA Calibration Manual³.

3. RESULTS

3.1. H_2CO , H_2^{13}CO , and $\text{H}_2\text{C}^{18}\text{O}$

We detected the double peak 6 cm formaldehyde maser in NGC 7538 IRS 1 in all nine epochs (six GBT observations, two WSRT, and one VLA run; Figure 2). In epoch 4 (July 17, 2009), we also observed five other HMSFRs in C-Band. The results of the observations are summarized in Table 3: column 1 lists the sources, columns 2 to 5 give the rms and line parameters (peak flux density, peak velocity, and FWHM), and column 6 gives the epochs of observation. The parameters of the absorption lines are presented in Table 4 (the absorption lines were fit simultaneously with the emission lines when detected, see Figure 3). We also detected the $1_{10} - 1_{11}$ (4.59309 GHz) transition of the H_2^{13}CO isotopologue in absorption, which is the equivalent quantum transition of the main 6 cm formaldehyde line (previous detections of this transition toward other regions are reported in e.g., Wilson et al. 1976; Henkel et al. 1982; Kutner et al. 1982). In the case of NGC 7538 IRS 1⁴, we found a hint of absorption in all epochs; the average spectra and line parameters are presented in Figure 4 and Table 5. Weak 4.59 GHz H_2^{13}CO isotopologue absorption was also detected toward G23.01–0.41, G25.83–0.18, G29.96–0.02, and IRAS 18566+0408 (Table 5). H_2^{13}CO and H_2CO absorption is seen at the same LSR velocities, which suggests similar gas distribution. No isotopologue absorption was detected in G23.71–0.20 (Figure 4). No 4.59 GHz H_2^{13}CO emission lines were detected. Emission overlapped with

² The WSRT is operated by ASTRON (Netherlands Institute for Radio Astronomy) with support from the Netherlands Foundation for Scientific Research (NWO).

³ <http://www.aoc.nrao.edu/~gtaylor/csource.html>, accessed on 2016 July 14th.

⁴ We note that all the absorption lines detected in the NGC 7538 IRS 1 pointing are likely tracing extended clouds and originate from absorption against all continuum sources within the GBT beam, not only the IRS 1 region.

Table 3. 6 cm Formaldehyde Masers

Source	rms	S_ν	V_{LSR}	FWHM	Epoch/Date
	(mJy)	(mJy)	(km s ⁻¹)	(km s ⁻¹)	
G23.01−0.41	7	... ¹	4/2009-July-17
G23.71−0.20 ²	8	71(8)	79.49(0.02)	0.43(0.05)	4/2009-July-17
G25.83−0.18 ²	10	104(8)	90.24(0.02)	0.48(0.04)	4/2009-July-17
G29.96−0.02 ²	14	120(20)	100.40(0.05)	1.1(0.2)	4/2009-July-17
IRAS 18566+0408 ²	5	16(6)	79.6(0.2)	1.3(0.6)	1/2008-May-05
	6	15(3)	79.2(0.1)	1.3(0.3)	4/2009-July-17
NGC 7538 IRS 1 ³	20	1295(20)	−57.95(0.09)	0.85(0.19)	1/2008-May-05
		661(20)	−60.22(0.09)	0.85(0.19)	
	16	1184(16)	−57.95(0.09)	0.95(0.19)	2/2009-May-18
		753(16)	−60.22(0.09)	0.76(0.19)	
	16	1215(16)	−57.83(0.09)	0.95(0.19)	3/2009-July-03
		715(16)	−60.20(0.09)	0.76(0.19)	
	16	1242(16)	−57.85(0.09)	0.95(0.19)	4/2009-July-17
		736(16)	−60.22(0.09)	0.76(0.19)	
	25	1177(25)	−57.81(0.09)	0.95(0.19)	5/2010-May-07
		812(25)	−60.18(0.09)	0.76(0.19)	
	28	1109(28)	−57.97(0.09)	1.04(0.19)	6/2011-May-31
		884(28)	−60.15(0.09)	0.76(0.19)	
	40	959(40)	−57.78(0.09)	0.95(0.19)	7/2014-December-07
		988(40)	−60.14(0.09)	0.47(0.19)	
	67	934(67)	−57.78(0.09)	0.95(0.19)	8/2015-May-29
		911(67)	−60.24(0.09)	0.76(0.19)	
	30	945(30)	−57.84(0.06)	1.03(0.12)	9/2015-June-28
		985(30)	−60.20(0.06)	0.73(0.12)	

¹ Emission was blended with absorption and no reliable measurement was possible (see Figure 3).

² Parameters were obtained from Gaussian fits (Figure 3). 1σ statistical errors from the fits are listed as uncertainty.

³ The masers in NGC 7538 IRS 1 deviated significantly from Gaussian profiles, thus, we report the peak channel flux density (spectrum rms reported as uncertainty), peak channel velocity (channel width listed as uncertainty), and full width at half maximum (two times the channel width reported as uncertainty). In the case of the GBT data (observing epochs 1 to 6), the H₂CO absorption given in Table 4 was subtracted from each spectrum before measuring the line parameters of the masers.

absorption of the 14.5 GHz H₂CO transition was detected in NGC 7538 IRS 1 and it will be discussed in a later work. We also report non-detections of the 13.78 GHz H₂¹³CO and 4.39 GHz H₂C¹⁸O transitions toward NGC 7538 IRS 1 (see Table 5).

3.2. CH₃OH and ¹³CH₃OH

We observed 12.2 GHz methanol masers in NGC 7538 IRS 1 in 2008 and 2010 (Figure 5, Table 6). Multiple velocity components were detected, and the flux density of the main peak (−56 km s⁻¹) slightly decreased between the two epochs. We also detected weak absorption (−12 mJy at −60 km s⁻¹, rms ∼ 3 mJy, Table 5) of the ¹³CH₃OH isotopologue (14.782212 GHz) toward NGC 7538 IRS 1 in two epochs (epochs 1 and 5, Ku-Band). This is the equivalent quantum transition of the main methanol isotope at 12.2 GHz. In addition, we detected two K-Band methanol transitions (20.171089 GHz and 20.970651 GHz) in three observing runs (2008, 2009, and 2010, Table 6). All methanol lines are shown in Figure 5. The 19.9 GHz methanol line was also detected but it will be discussed in a later paper.

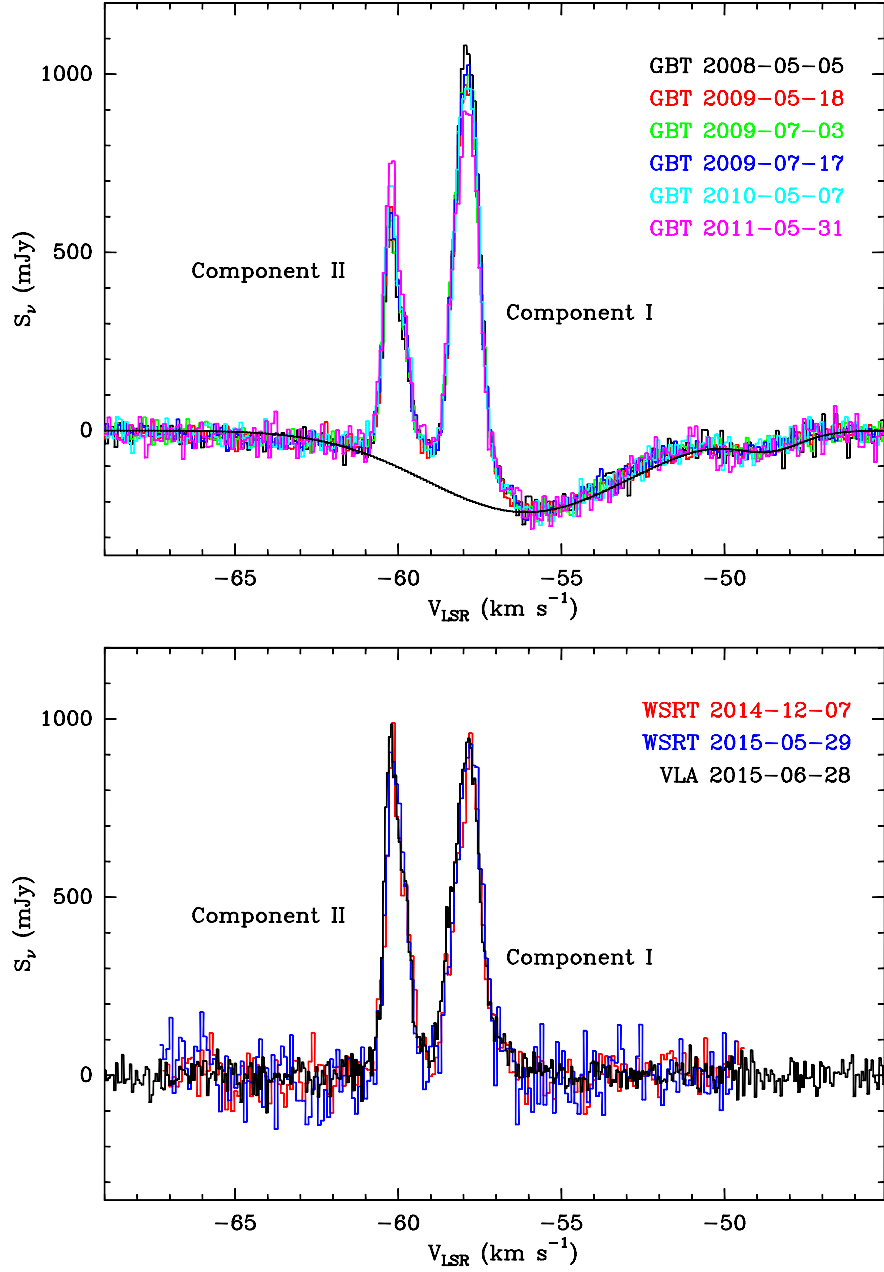


Figure 2. Spectra of the 6 cm formaldehyde masers obtained towards NGC 7538 IRS 1 in the nine observing epochs. *Top panel:* the 2008–2011 GBT observations. The fit to the averaged formaldehyde double peaked absorption is shown. The consistency in the absorption profiles detected with the GBT (which are not expected to change because of their extended angular size) shows that the observed variability of the masers is not caused by calibration errors. *Lower panel:* the 2014 and 2015 observations were obtained with the WSRT and VLA (no formaldehyde absorption was detected within the solid angle of the masers).

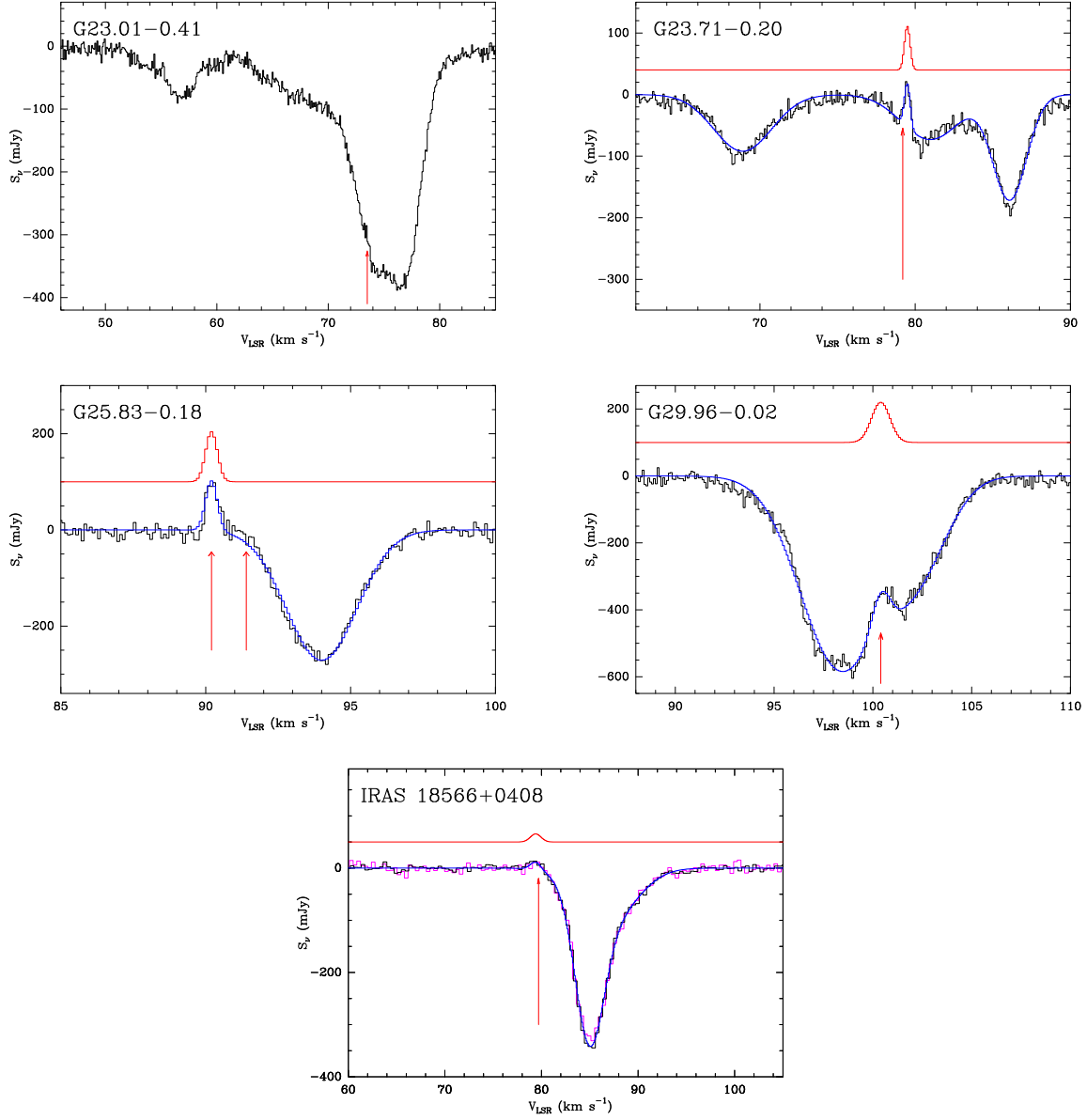


Figure 3. Spectra of 6 cm formaldehyde masers toward the other five sources in our sample. All sources were observed on July 17, 2009 (black spectra, epoch 4); IRAS 18566+0408 was also observed in May 5, 2008 (epoch 1; pink spectrum). Red arrows indicate the velocity of previously reported 6 cm formaldehyde masers in the regions (Araya et al. 2008, 2004b; Pratap et al. 1994). The blue curves show Gaussian fits to the emission and absorption profiles (a reliable fit of the maser was not possible in the case of G23.01–0.41). The red curves show the Gaussian fit of the maser line (the red fits were offset vertically for clarity).

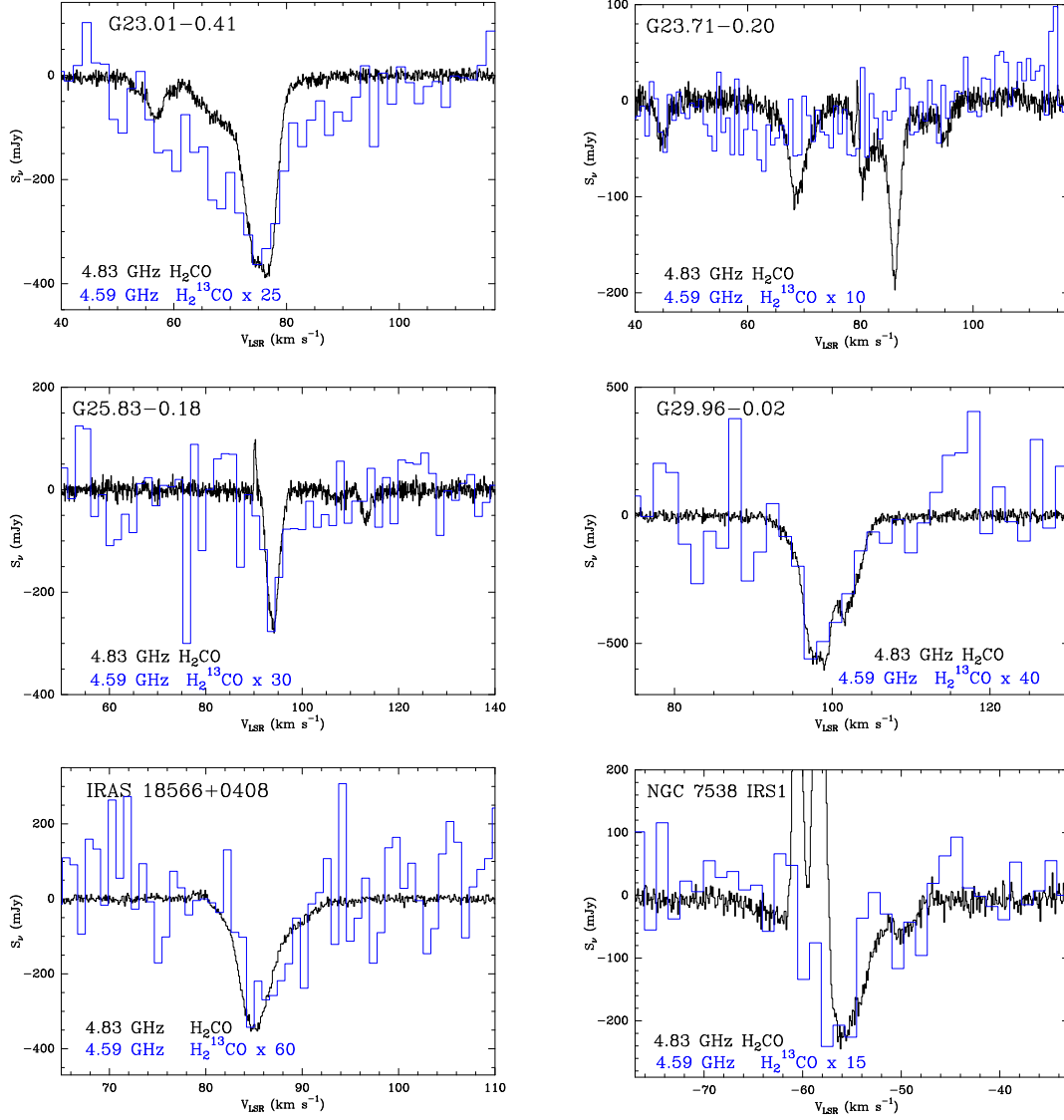


Figure 4. H_2^{13}CO isotopologue spectra (4.59 GHz, blue) obtained toward the six sources in our sample overlapped with the spectra of the main isotopologue (4.83 GHz, black). The H_2^{13}CO spectra were multiplied by an arbitrary factor to facilitate comparison with the main isotopologue. The isotopologue spectra were smoothed to different channel widths (see Table 1).

Table 4. 6 cm Formaldehyde Absorption

Source	rms	S_ν	V_{LSR}	FWHM
	(mJy)	(mJy)	(km s ⁻¹)	(km s ⁻¹)
G23.01−0.41	7	−21(1)	4.9(0.1)	5.2(0.3)
		−45(8)	56.2(0.3)	6.4(0.7)
		−39(8)	56.9(0.1)	2.1(0.4)
		−90(4)	69.3(0.7)	10.0(1.3)
		−370(20)	75.71(0.05)	5.6(0.1)
G23.71−0.20	8	−43(3)	44.84(0.06)	2.2(0.2)
		−92(2)	68.89(0.05)	4.4(0.1)
		−73(3)	80.98(0.09)	4.4(0.2)
		−170(3)	86.09(0.03)	2.57(0.07)
		−21(2)	91.0(0.3)	4.9(1.3)
G25.83−0.18	11	−36(4)	95.1(0.1)	2.0(0.3)
		−42(3)	11.11(0.07)	1.9(0.2)
		−271(3)	93.97(0.02)	2.86(0.04)
		−19(2)	107.2(0.2)	3.6(0.5)
		−57(3)	113.29(0.06)	2.3(0.1)
G29.96−0.02	14	−580(10)	6.92(0.02)	1.23(0.04)
		−170(10)	8.50(0.07)	1.3(0.2)
		−65(5)	49.95(0.07)	2.0(0.2)
		−19(3)	57.7(0.4)	4.2(0.8)
		−173(4)	66.95(0.03)	2.46(0.07)
IRAS 18566+0408 ¹	3	−570(10)	98.31(0.09)	4.7(0.1)
		−270(10)	102.2(0.1)	3.7(0.2)
		−34(3)	21.0(0.1)	1.4(0.2)
		−24(3)	23.6(0.1)	1.5(0.2)
		−237(17)	87.1(0.1)	4.6(0.2)
NGC 7538-IRS 1 ²	13	−58(16)	88.9(0.6)	8.7(0.7)
		−229(4)	−56.83(0.08)	7.3(0.1)
		−47 (5)	−49.4 (0.1)	2.3 (0.3)

Line parameters from Gaussian fits; 1σ statistical errors from the fits are listed as uncertainty.

¹ Average of two GBT spectra: epochs 1 and 4.

² Average of GBT spectra obtained in position switching mode. As mentioned in section 3.1, absorption features in the direction of NGC 7538-IRS 1 of all species reported in this work are likely tracing extended clouds seen in absorption against some or all continuum regions within the GBT beam.

3.3. H₂O

We conducted observations of the 22.2 GHz water transition in NGC 7538 IRS 1 (2008, 2009, and 2010; Table 7, Figure 6). Our data show decreasing intensity of the main component (−58.2 km s⁻¹) and highly variable weaker components (Figure 6). We also detected water absorption at LSR velocity of −50 km s⁻¹, which was mostly masked by a variable water maser in the May 2009 spectrum (green, Figure 6). The velocity of this water absorption line is similar to the velocity of a weak 6 cm formaldehyde absorption component (Table 4).

Table 5. Line Parameters of Isotopologues

Source	Molecule	Frequency (GHz)	rms (mJy)	S_ν (mJy)	V_{LSR} (km s ⁻¹)	FWHM (km s ⁻¹)	Epoch/Date
G23.01–0.41	H ₂ ¹³ CO	4.5930885	2	−11(1)	72.5(0.7)	21(2)	4/2009-July-17
G23.71–0.20	H ₂ ¹³ CO	4.5930885	3	4/2009-July-17
G25.83–0.18	H ₂ ¹³ CO	4.5930885	2	−8(2)	94.0(0.8)	5(2)	4/2009-July-17
G29.96–0.02	H ₂ ¹³ CO	4.5930885	4	−13(2)	98.9(0.5)	7(1)	4/2009-July-17
IRAS 18566+0408	H ₂ ¹³ CO	4.5930885	3	−6(1)	86.2(0.3)	6(1)	average ¹
NGC 7538 IRS 1	¹³ CH ₃ OH	14.7822120	3	−12(3)	−60.8(0.5)	5(1)	1/2008-May-05
			4	−13(3)	−59.2(0.4)	4(1)	5/2010-May-07
	H ₂ ¹³ CO	4.5930885	3	−16(3)	−56.7(0.3)	4(1)	average ²
	H ₂ ¹³ CO	13.7788041	6	average ¹
	H ₂ C ¹⁸ O	4.3887970	7	average ²

Line parameters from Gaussian fits; 1 σ statistical errors from the fits are listed as uncertainty.

¹ Average of two epochs, see Tables 1 and 2.

² Average of GBT spectra obtained in position switching mode.

3.4. Radio Recombination Lines

We observed four RRLs in C-Band (H109 α , H137 β , H141 β , and H174 δ) and one in K-Band (H86 β) toward NGC 7538 IRS 1 (Figure 7, Table 8). The HPBW of our C- and K-band observations is large enough to not only include emission from NGC 7538 IRS 1, but also from the ultracompact HII regions labeled A and C by Wood & Churchwell (1989) (also known as IRS 2 and IRS 3, e.g., Sewilo et al. 2004), and the compact HII region Sharpless 158 (e.g., Luisi et al. 2016). This is evident because the RRLs we detected are narrower than the RRLs in NGC 7538 IRS 1 (e.g., Gaume et al. 1995; Sewilo et al. 2004, Keto et al. 2008). We also report detection of H137 β and H141 β toward G23.01–0.41, G23.71–0.20, and G29.96–0.02 (Figure 7). In all cases, we measured full width at half maximum (FWHM) values between 20 and 35 km s⁻¹ and found no significant flux density variability within the rms of the observations (Table 8, Figure 7). The consistency between different epochs exemplifies the reliability of GBT observations for multi-year monitoring studies of spectral lines.

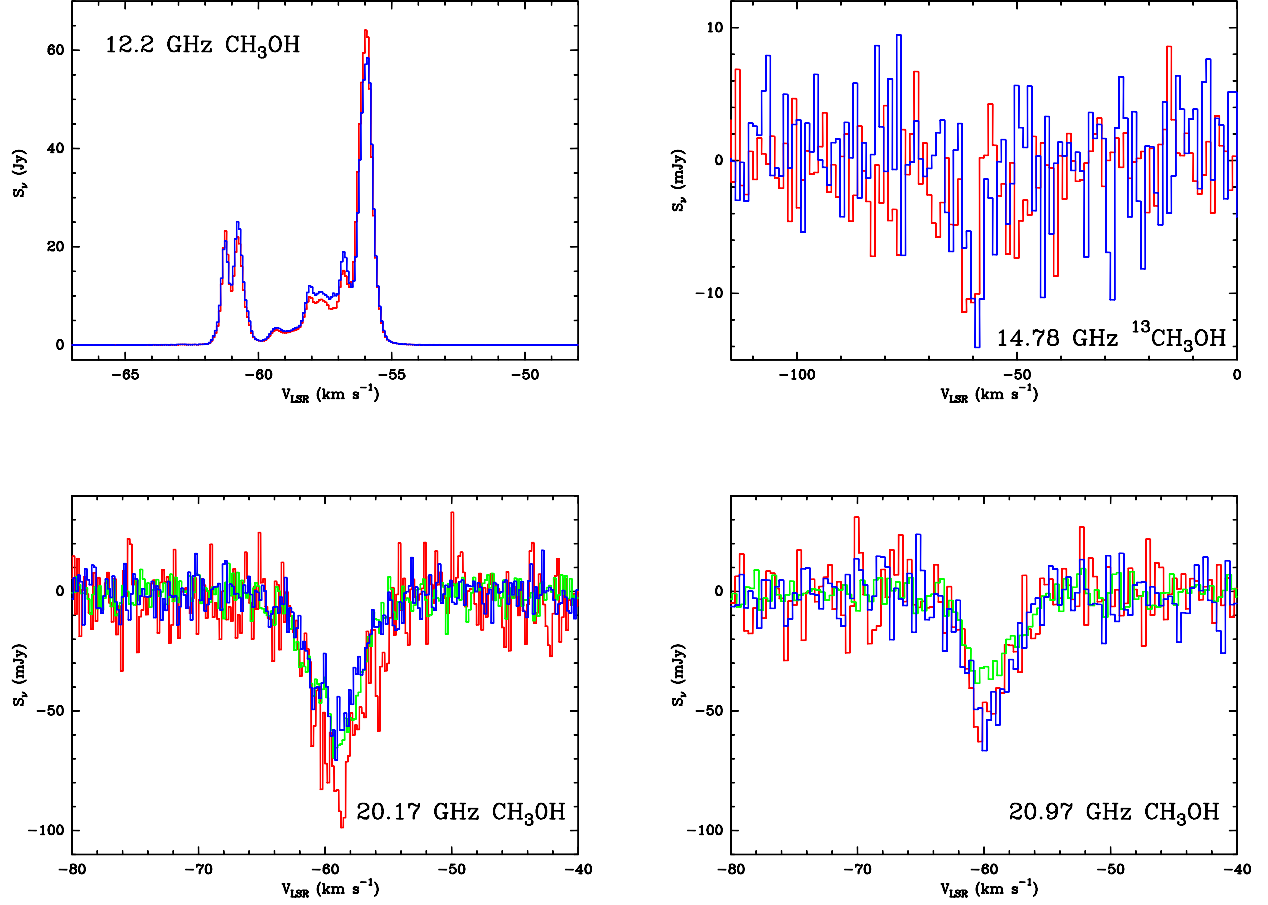


Figure 5. Methanol spectra obtained towards NGC 7538 IRS 1. The spectra of the strong 12.2 GHz methanol masers are shown in the upper left panel, $^{13}\text{CH}_3\text{OH}$ isotopologue absorption is shown in the upper right panel, and methanol absorption spectra from two other transitions are shown in the lower panels. Red, green, and blue spectra show data from 2008 (epoch 1), 2009 (epoch 2), and 2010 (epoch 5), respectively (not all lines were observed in all epochs).

Table 6. Line Parameters of Methanol Transitions Toward NGC 7538 IRS 1

Frequency (GHz)	rms (mJy)	S_ν (Jy)	V_{LSR} (km s ⁻¹)	Linewidth (km s ⁻¹)	Epoch/Date
12.1785970	15	23.247(0.015)	-61.23(0.08)	1.13(0.15)	1/2008-May-05
		22.033(0.015)	-60.78(0.08)	1.05(0.15)	
		3.037(0.015)	-59.35(0.08)	0.98(0.15)	
		9.797(0.015)	-58.08(0.08)	1.20(0.15)	
		9.280(0.015)	-57.63(0.08)	0.68(0.15)	
		15.136(0.015)	-56.80(0.08)	0.75(0.15)	
		64.089(0.015)	-55.97(0.08)	2.03(0.15)	
	21	21.181(0.021)	-61.23(0.08)	0.98(0.15)	5/2010-May-07
		25.113(0.021)	-60.78(0.08)	1.05(0.15)	
		3.517(0.021)	-59.28(0.08)	0.98(0.15)	
		12.076(0.021)	-58.08(0.08)	1.13(0.15)	
		10.834(0.021)	-57.63(0.08)	0.53(0.15)	
		18.992(0.021)	-56.80(0.08)	0.83(0.15)	
		58.486(0.021)	-55.90(0.08)	1.95(0.15)	
14.782212	3	-0.012(0.003)	-60.8(0.5)	4(1)	1/2008-May-05
	4	-0.013(0.003)	-59.2(0.4)	3.7(0.9)	5/2010-May-07
20.1710890	13	-0.078(0.004)	-58.8(0.1)	4.7(0.2)	1/2008-May-05
	5	-0.059(0.001)	-59.10(0.06)	4.7(0.1)	2/2009-May-18
	7	-0.053(0.002)	-59.12(0.08)	4.8(0.2)	5/2010-May-07
20.9706510	11	-0.053(0.005)	-59.7(0.2)	3.9(0.4)	1/2008-May-05
	4	-0.035(0.002)	-59.5(0.1)	4.6(0.3)	2/2009-May-18
	9	-0.054(0.003)	-59.6(0.1)	4.1(0.3)	5/2010-May-07

The 12.2 GHz CH₃OH spectra showed multiple overlapped velocity components which could not be reliably fit using Gaussians, thus, we report the peak flux density (spectrum rms reported as uncertainty), velocity of the peak channel (channel width listed as uncertainty), and the linewidth measured between local minima of overlapping lines (two times the channel width reported as uncertainty). All other transitions were fit with Gaussian functions, 1σ statistical errors from the fit are shown in parentheses; the linewidth corresponds to the FWHM.

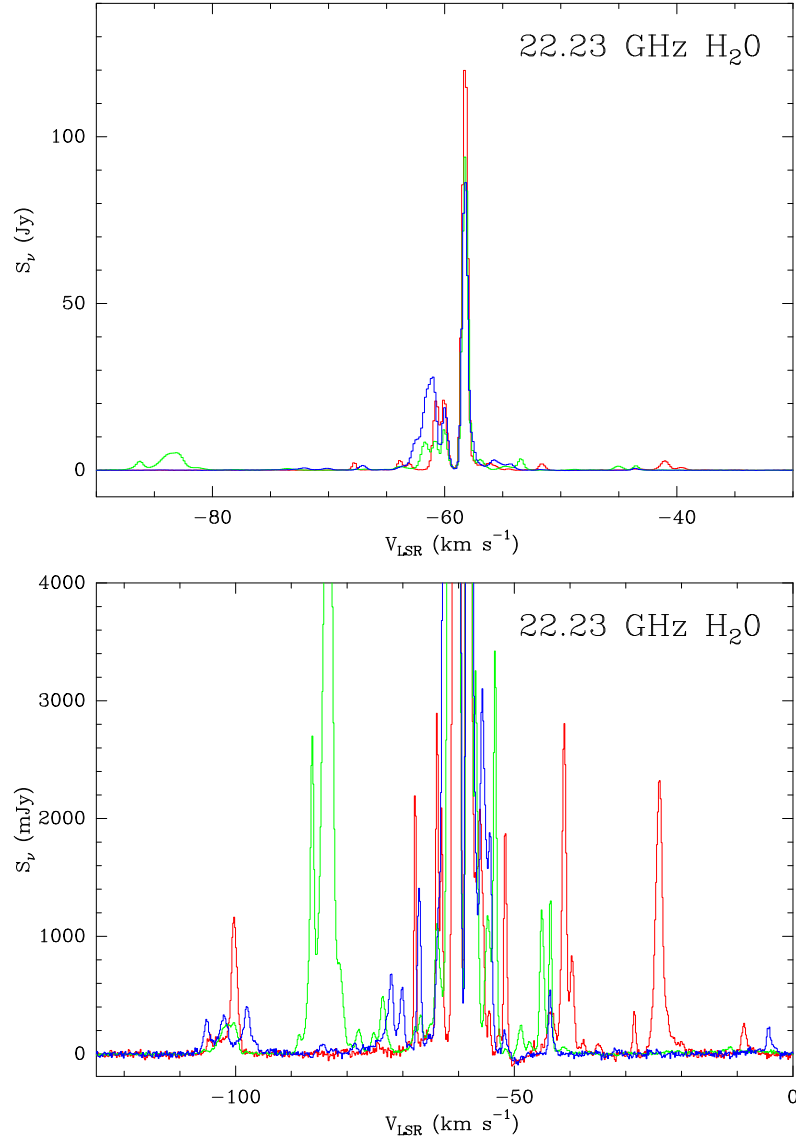


Figure 6. The figure shows H₂O spectra towards NGC 7538 IRS 1 from May 2008 (epoch 1; red), May 2009 (epoch 2; green), and May 2010 (epoch 5; blue). The lower panel shows a zoom-in of the weak features (note the change in units to mJy) and displays a broader velocity range than the upper panel. A decrease in the flux density of the main component (-58.2 km s^{-1}) is seen in the upper panel. We also detected water absorption at about -50 km s^{-1} .

Table 7. Line Parameters of Water Masers Toward NGC 7538 IRS 1

S_ν (Jy)	V_{LSR} (km s ⁻¹)	FWHM (km s ⁻¹)	Epoch/Date
0.14(0.02)	-104.69(0.08)	1.0(0.2)	1/2008-May-05
0.14(0.02)	-103.3(0.1)	1.0(0.4)	
0.14(0.02)	-102.0(0.2)	1.1(0.4)	
1.14(0.02)	-100.24(0.01)	1.24(0.03)	
0.07(0.01)	-74.3(0.1)	1.6(0.3)	
0.108(0.005)	-68.86(0.02)	0.86(0.06)	
2.33(0.07)	-67.77(0.01)	0.43(0.02)	
2.79(0.06)	-63.84(0.01)	0.51(0.01)	
1.88(0.07)	-63.04(0.01)	0.52(0.02)	
20.7(0.4)	-60.73(0.01)	0.59(0.02)	
21.2(0.5)	-60.01(0.01)	0.52(0.02)	
126(3)	-58.24(0.01)	0.56(0.02)	
1.1(0.2)	-57.14(0.09)	0.6(0.2)	
2.01(0.05)	-56.14(0.04)	1.31(0.08)	
0.39(0.02)	-54.49(0.01)	0.59(0.04)	
0.19(0.02)	-52.65(0.04)	0.9(0.1)	
1.95(0.05)	-51.61(0.01)	0.61(0.02)	
-0.08(0.04)	-49.5(0.5)	2(1)	
0.11(0.01)	-46.46(0.03)	0.38(0.06)	
0.36(0.03)	-43.35(0.07)	1.8(0.2)	
2.74(0.04)	-41.03(0.01)	0.89(0.01)	
0.82(0.03)	-39.67(0.02)	0.98(0.04)	
0.093(0.007)	-37.71(0.05)	1.3(0.1)	
0.088(0.009)	-34.89(0.05)	1.0(0.1)	
0.37(0.02)	-28.45(0.01)	0.57(0.03)	
2.28(0.04)	-24.01(0.02)	1.42(0.04)	
0.21(0.04)	-22.1(0.2)	1.4(0.5)	
0.245(0.008)	-8.79(0.02)	1.02(0.05)	2/2009-May-18
0.043(0.007)	-7.2(0.2)	1.4(0.4)	
0.033(0.002)	-105.51(0.06)	1.7(0.2)	
0.245(0.004)	-101.62(0.06)	2.9(0.1)	
0.14(0.01)	-100.10(0.02)	1.06(0.09)	
0.165(0.008)	-88.49(0.03)	1.09(0.08)	
2.5(0.1)	-86.27(0.03)	0.96(0.06)	
5.44(0.09)	-83.45(0.02)	2.09(0.05)	
0.6(0.1)	-81.0(0.1)	0.9(0.3)	
0.086(0.004)	-79.55(0.04)	1.0(0.1)	
0.209(0.004)	-77.92(0.01)	1.18(0.03)	
0.18(0.02)	-75.27(0.05)	1.0(0.1)	
0.47(0.01)	-73.54(0.02)	1.28(0.05)	
0.041(0.002)	-69.40(0.06)	1.5(0.2)	
0.220(0.007)	-67.64(0.08)	1.7(0.2)	
0.32(0.01)	-66.83(0.03)	1.4(0.1)	
0.25(0.02)	-65.1(0.1)	1.5(0.3)	
0.8(0.5)	-63.91(0.04)	0.7(0.1)	

Table 7 continued on next page

Table 7 (*continued*)

S_ν (Jy)	V_{LSR} (km s ⁻¹)	FWHM (km s ⁻¹)	Epoch/Date
0.59(0.1)	-63.2(0.4)	1.3(0.9)	
8.3(0.3)	-61.66(0.02)	0.85(0.05)	
8.6(0.3)	-60.80(0.01)	0.53(0.04)	
12.0(0.3)	-60.00(0.01)	0.59(0.02)	
96.1(0.8)	-58.225(0.003)	0.580(0.007)	
3.2(0.7)	-57.0(0.1)	1.1(0.3)	
1.16(0.03)	-54.70(0.02)	1.29(0.05)	
3.35(0.04)	-53.43(0.01)	0.62(0.01)	
-0.04(0.01)	-50.49(0.07)	0.5(0.2)	
0.242(0.005)	-48.84(0.01)	1.02(0.02)	
1.22(0.02)	-45.02(0.01)	0.88(0.01)	
1.35(0.02)	-43.51(0.01)	0.56(0.01)	
0.055(0.003)	-41.14(0.05)	1.9(0.1)	
0.055(0.003)	-11.38(0.05)	1.6(0.1)	
0.04(0.02)	-107.13(0.09)	0.5(0.2)	5/2010-May-07
0.27(0.01)	-105.13(0.03)	1.39(0.06)	
0.304(0.008)	-102.17(0.03)	1.96(0.08)	
0.24(0.02)	-97.94(0.02)	0.86(0.08)	
0.18(0.02)	-98.09(0.07)	3.3(0.3)	
0.083(0.008)	-84.43(0.07)	1.3(0.2)	
0.085(0.007)	-78.65(0.05)	1.2(0.1)	
0.21(0.03)	-72.4(0.3)	4.3(0.6)	
0.46(0.03)	-72.13(0.03)	0.88(0.08)	
0.46(0.04)	-70.12(0.03)	0.84(0.09)	
0.05(0.02)	-68.2(0.9)	1.6(2)	
1.36(0.04)	-67.06(0.01)	0.79(0.03)	
1.3(0.2)	-63.4(0.3)	1.4(0.5)	
7.9(0.9)	-62.49(0.03)	0.76(0.08)	
22.9(0.7)	-61.50(0.03)	0.89(0.09)	
20(3)	-60.91(0.02)	0.60(0.03)	
18.6(0.2)	-59.97(0.01)	0.58(0.01)	
87(2)	-58.25(0.01)	0.53(0.01)	
6.9(0.7)	-57.6(0.1)	0.8(0.2)	
2.91(0.06)	-55.69(0.02)	1.32(0.06)	
1.68(0.08)	-54.34(0.03)	0.88(0.06)	
0.18(0.07)	-51.7(0.2)	0.9(0.4)	
-0.070(0.008)	-49.4(0.1)	1.5(0.2)	
0.17(0.02)	-47.5(0.2)	0.3(0.3)	
0.46(0.03)	-43.61(0.07)	0.49(0.02)	
0.14(0.02)	-43.23(0.08)	1.1(0.1)	
0.035(0.009)	-31.38(0.06)	0.4(0.1)	
0.025(0.009)	-25.7(0.3)	1.1(0.7)	
0.04(0.01)	-24.38(0.06)	0.4(0.1)	
0.05(0.02)	-7.8(0.1)	0.6(0.3)	
0.20(0.02)	-4.30(0.05)	1.2(0.1)	

Line parameters from Gaussian fits; 1σ statistical errors from the fit are shown in parentheses. The rms of the spectra are: 19 mJy (1/2008-May-05), 7 mJy (2/2009-May-18), 10 mJy (5/2010-May-07).

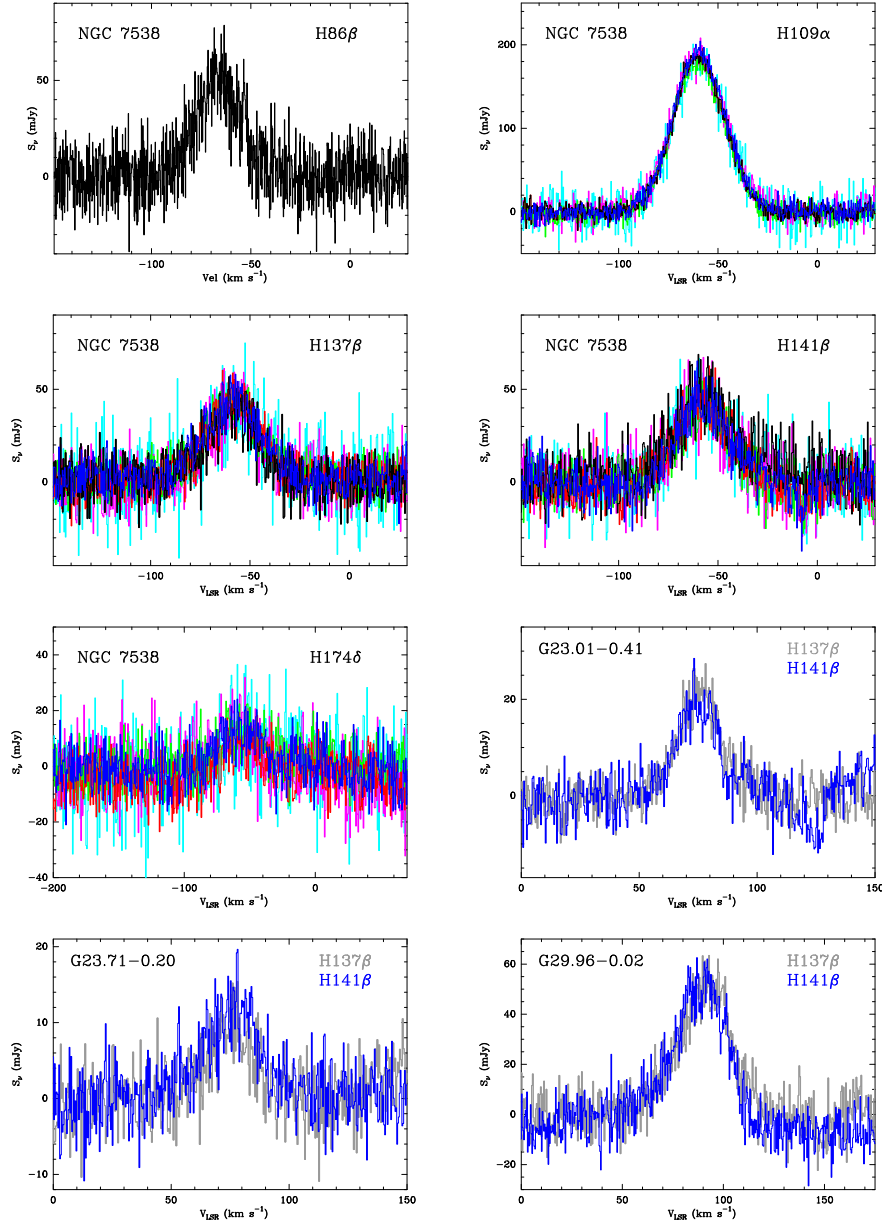


Figure 7. Radio recombination lines detected in this project. The NGC 7538 panels show specific radio recombination line transitions, and different colors represent different observing epochs: May 2008 (epoch 1; black), May 2009 (epoch 2; red), July 2009 (epoch 3; green), July 2009 (epoch 4; blue), May 2010 (epoch 5; pink), and May 2011 (epoch 6; magenta). Not all lines were observed in all epochs (see Table 1). The panels of G23.01–0.41, G23.71–0.20, and G29.96–0.02 show two different recombination line transitions (H137 β in grey; H141 β in blue) that were observed in epoch 4 (July 17, 2009).

Table 8. Radio Recombination Lines

Source	RRL	Frequency (GHz)	rms (mJy)	S_ν (mJy)	V_{LSR} (km s $^{-1}$)	FWHM (km s $^{-1}$)	Epoch/Date
G23.01−0.41	H137 β	5.00503238	4	22(1)	75.6(0.3)	20.8(0.7)	4/2009-July-17
	H141 β	4.59384760	4	19(1)	74.5(0.4)	20.1(0.9)	
G23.71−0.20	H137 β	5.00503238	2	12(1)	75.9(0.6)	28(2)	4/2009-July-17
	H141 β	4.59384760	3	10(1)	75.3(0.7)	20(2)	
G29.96−0.02	H137 β	5.00503238	7	53(1)	88.5(0.3)	27.4(0.8)	4/2009-July-17
	H141 β	4.59384760	8	51(1)	91.0(0.4)	30.2(0.8)	
NGC 7538	H86 β	19.97816269	13	51(2)	−66.5(0.4)	26.2(0.9)	1/2008-May-05
	H109 α	5.00892233	7	198(3)	−59.3(0.2)	33.9(0.5)	1/2008-May-05
			6	187(1)	−59.6(0.1)	30.1(0.2)	2/2009-May-18
			7	180(1)	−59.8(0.1)	30.2(0.2)	3/2009-July-03
			8	192(1)	−59.5(0.1)	30.7(0.2)	4/2009-July-17
			8	185(2)	−59.7(0.2)	31.7(0.3)	5/2010-May-07
			17	184(3)	−59.2(0.2)	30.5(0.5)	6/2011-May-31
	H137 β	5.00503238	9	39(2)	−58.8(0.6)	30(1)	1/2008-May-05
			6	42(1)	−58.2(0.4)	31(1)	2/2009-May-18
			7	41(1)	−58.5(0.4)	31(1)	3/2009-July-03
			8	42(1)	−58.6(0.4)	32(1)	4/2009-July-17
			8	43(2)	−57.6(0.6)	30(1)	5/2010-May-07
			16	39(2)	−57(1)	34(2)	6/2011-May-31
	H141 β	4.59384760	10	42(2)	−56.4(0.7)	34(2)	1/2008-May-05
			8	46(1)	−58.0(0.5)	33(1)	2/2009-May-18
			9	41(1)	−57.8(0.5)	30(1)	3/2009-July-03
			7	46(1)	−57.3(0.5)	32(1)	4/2009-July-17
			10	43(2)	−58.1(0.7)	27(2)	5/2010-May-07
			14	42(2)	−58.1(0.8)	32(2)	6/2011-May-31
	H174 δ	4.82617096	7	12(1)	−57(2)	37(4)	2/2009-May-18
			6	12(1)	−56(2)	34(4)	3/2009-July-03
			6	15(1)	−59(1)	36(3)	4/2009-July-17
			9	16(2)	−59(2)	33(4)	5/2010-May-07
13			11(3)	−54(3)	25(7)	6/2011-May-31	

Radio recombination lines frequencies were obtained from Splatalogue. Line parameters from Gaussian fits; 1σ statistical errors from the fit are shown in parentheses.

4. DISCUSSION

4.1. Formaldehyde

4.1.1. H_2CO Masers in NGC 7538 IRS 1

In contrast to many other astrophysical masers, the two individual 6 cm formaldehyde maser velocity components in NGC 7538 IRS 1 have persisted for four decades. Figure 8 shows the light-curve of these masers, including the measurements reported in this work and data from the literature. Our data confirm the statement by Araya et al. (2007b) that the flux density rate of change of the brighter maser (Component I) decreased approximately from 2004. Specifically, our light curve indicates that Component I reached a maximum flux density sometime near 2004, and its flux density has been decreasing ever since, while the flux density of Component II started increasing after 1996.

As noted by Araya et al. (2007b), both maser components showed little variability from their detection in 1974 until the early 1980s, when Component I showed an increase in flux density of the order of 30 mJy year^{-1} , while Component II showed no variability until sometime after 1996, when a similar variability slope was detected (see Figure 8). Araya et al. (2007b) mentioned the possibility that some type of perturbation could have passed through one maser region causing the variability, and then reached Component II ~ 14 years later, triggering a similar variability behavior with a time delay. Our observations show that the similar variability of both maser components has indeed continued (Figure 8). However, the hypothesis that some type of propagating phenomenon (e.g., a shock front passing through the medium) is responsible for the variability of both maser components seems now unlikely because one would expect some change in the velocity and/or linewidth of the masers, but our data do not show a significant change in kinematic parameters. Thus, the similar variability may not be caused by a single triggering mechanism that affected both maser regions with a time delay, but rather by similar properties of two independent maser clouds. For instance, the variability could be attributed to a change in the maser cloud physical depth as a function of time (i.e., a change in the amplification/gain path-length through a uniformly pumped medium in our line-of-sight). In a simple amplification model, the maser region can be assumed to have an ellipsoidal shape, spin as a solid body with constant angular momentum (giving velocity coherence along the line-of-sight), and constant pumping. As time passes, the rotation would change the maximum line-of-sight amplification path through the maser cloud $s(t)$:

$$s(t) = \frac{2ab}{\sqrt{[a \sin(\omega(t-t_0))]^2 + [b \cos(\omega(t-t_0))]^2}}, \quad (1)$$

where a , b , ω are the semimajor axis, semiminor axis, and angular velocity, respectively. This change in amplification path would modify the maser's flux density because the maser gain would change as $\tau_\nu \propto s(t)$ (see Figure 9).

The black curve in Figure 8 shows the result of fitting the light-curve of maser Component I to this simple rotating ellipsoidal model. The model assumes unsaturated maser amplification and that the maximum line-of-sight segment across the ellipsoid produces all observed flux density (1D approximation). This is clearly a zero-order approximation because contributions from other lines-of-sight across the ellipsoid are neglected. Nevertheless, it is a useful model to discuss how changes in the maser depth could explain the observed variability. In the context of this model, our data indicate that the ellipsoid was observed near when its major axis was in our line-of-sight. Thus, assuming a prolate geometry, the maximum line-of-sight gain length would dominate the amplification, which justifies the use of the 1D approximation. The model shown in Figure 8 (black curve) corresponds to a semi-major axis of $\sim 250 \text{ AU}$, an aspect ratio between the major and minor axes of ~ 10 , a rotation period of ~ 1500 years, and its major axis was in the direction of our line-of-sight in 2006.

We note that the model has a degeneracy in the physical size of the ellipsoid, for instance, the maser cloud could be larger (e.g., $\sim 2000 \text{ AU} \times 200 \text{ AU}$) if the pumping mechanism were less efficient. Hoffman et al. (2003) reported a projected size of Component I of $\approx 200 \text{ AU}$, and assumed a gain length of $\approx 2000 \text{ AU}$ in their analysis. Thus, the physical dimensions of the ellipsoid used in our model are similar to their observed values. Moreover, Hoffman et al. (2003) reported a velocity gradient of $1900 \text{ km s}^{-1} \text{ pc}^{-1}$, which would correspond to one complete revolution of the ellipsoid in $\approx 3000 \text{ yr}$. Thus, the line-of-sight ray through the ellipsoid would exhibit maximal and minimal path lengths every 1500 yr which is similar to the results of our model.

The most interesting aspect of this simple model is that the same curve used to fit the data of Component I also fits well the light-curve of Component II by simply assuming a time-shift of 15 years (blue dashed curve, Figure 8).⁵

⁵ However, we note that the flux density of Component II measured in 2014 and 2015 seems lower than expected from the model.

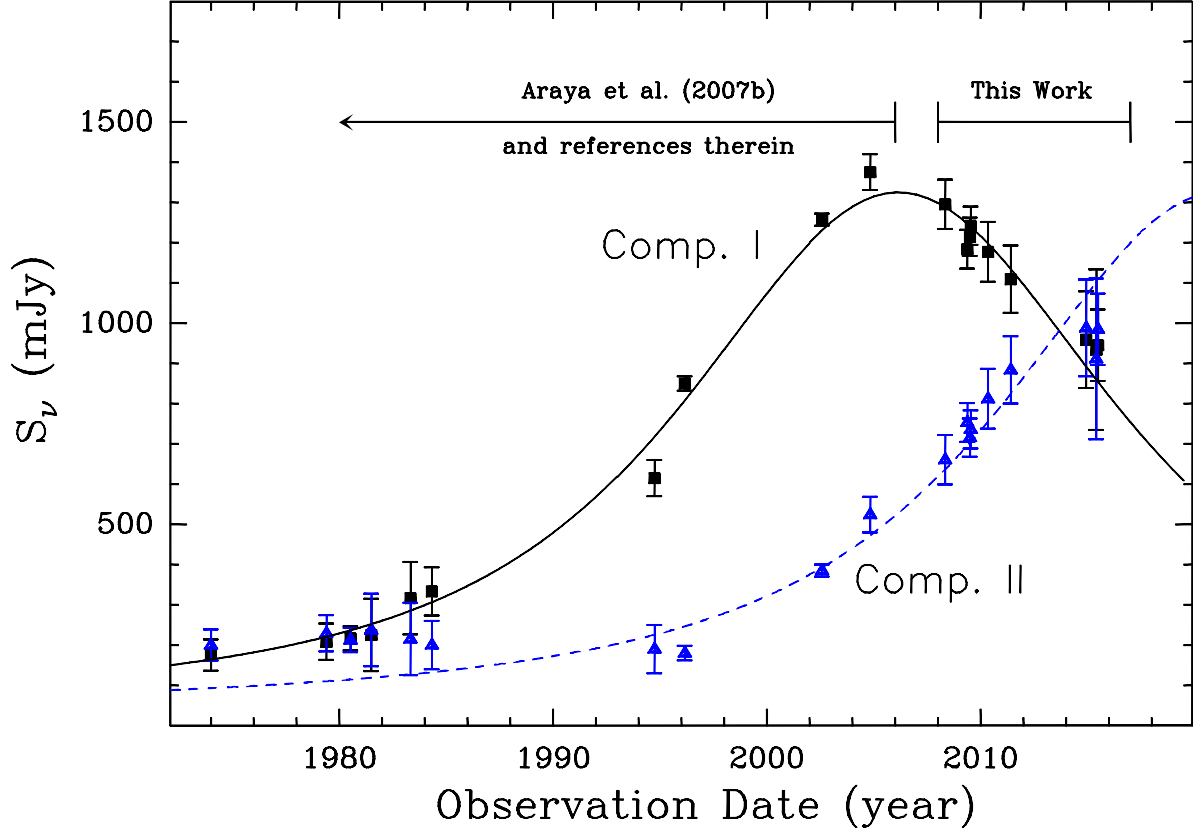


Figure 8. Light curve of the two formaldehyde maser components in NGC 7538 IRS 1; $\pm 3\sigma$ error bars are shown. The black line shows a fit of the Component I data by assuming that the maser is generated by a spinning-ellipsoidal unsaturated maser region (see Section 4.1.1). The blue dashed curve is the same black fit shifted by 15 years to highlight the similar variability behavior of both maser components and the possibility that changes in the line-of-sight amplification path through the maser clouds could be responsible for the observed variability.

In this interpretation, the similar variability profile of both maser regions is not connected or triggered by an external event with a time delay, but rather is a consequence of both maser regions having similar physical shapes and overall velocity gradients. However, it should be clear that the model is only a simple approximation to the current data. The rotation period of the ellipsoid is very long with respect to the sampling time ($> 1,000$ years vs 40 years), thus, it is highly unlikely that two unrelated maser clouds are almost perfectly oriented with their major axes in our line-of-sight with less than a few decades difference. Instead, the model simply suggests that the projected line-of-sight depth can be fit by an ellipsoidal morphology over the period of observations.

Recently, [Chen et al. \(2017\)](#) report observations of the 6 cm formaldehyde masers in NGC 7538 obtained with the 65 m Shanghai Tianma Radio Telescope (TMRT) in 2016 March and April. They report peak flux densities of 1.314 Jy (Component I) and 1.434 Jy (Component II), i.e., they found that by 2016, the flux density of Component II was greater than Component I, which is qualitatively consistent with the extrapolation of our data as shown in Figure 8. However, the flux densities reported by [Chen et al. \(2017\)](#) are greater than the expected values from extrapolation of the data reported here. It is unclear if this discrepancy is due to significant deviations from the extrapolated trends, or whether the flux densities reported by [Chen et al. \(2017\)](#) were overestimated. Follow up observations within the next 5 to 10 years are required to explore deviations from the long-term variability shown in Figure 8, to investigate

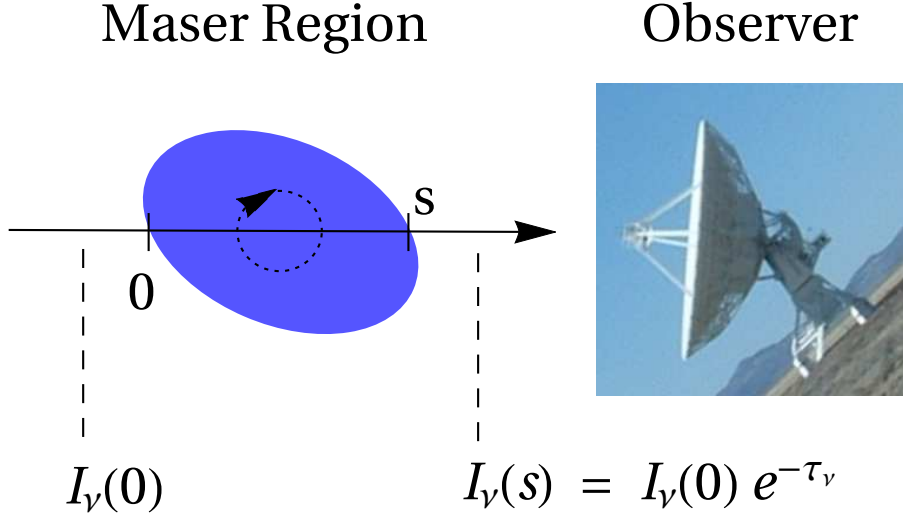


Figure 9. Simple model used to explain the observed variability. As the maser region slowly rotates, a different amplification path ($0 \rightarrow s$) results in a change in the maser gain (τ_ν), and thus, a change in the observed intensity.

symmetry in the variability profiles before and after maxima, and similarities between the light-curves of Components I and II. Such data are needed to develop a more realistic 3D model of the maser regions.

4.1.2. H_2CO Masers: Other Sources

As mentioned in Section 2.1, in addition to NGC 7538 IRS 1, five other formaldehyde maser sources were observed on 2009 July 17 (Table 2). Here we discuss the observations in the context of previous formaldehyde maser detections:

G23.01–0.41: is a region of active high-mass star formation at the distance 4.6 kpc (Brunthaler et al. 2009) in the Scutum constellation. The bolometric luminosity of G23.01–0.41 is $4 \times 10^4 L_\odot$ (Sanna et al. 2014b). Clear outflow activity is revealed by ^{12}CO observations (Furuya et al. 2008) and by intense $4.5 \mu m$ excess emission from a hot molecular core (HMC; Araya et al. 2008; Cyganowski et al. 2009). A weak (≈ 50 mJy beam $^{-1}$) formaldehyde maser was detected towards the HMC by Araya et al. (2008). As shown in Figure 3, upper left panel (red arrow), this maser is blended with stronger formaldehyde absorption at ~ 76 km s $^{-1}$ and weaker and broader one at ~ 69 km s $^{-1}$. The presence of formaldehyde absorption in this region is well known (e.g., Downes et al. 1980), and a double peak absorption profile has also been seen in OH (Sanna et al. 2014b). Given the overlapping absorption lines, a reliable measurement of the maser’s line parameters is not possible. Based on the asymmetry observed in the spectrum, we estimate a maser peak flux density of the order of 6σ (40 mJy), which is similar to the flux density of the maser detected in 2006 (Araya et al. 2008). We conclude that no significant variability of the maser is found between the 2006 and 2010 epochs.

Chen et al. (2017) also report observations of the formaldehyde maser. Even though they did not explicitly discuss variability of this source, Chen et al. (2017) list line parameters of the maser in their Table 1 and show the spectrum after removing the absorption in their Figure 1. However, the line they report is excessively broad (1.38 km s $^{-1}$ versus 0.4 km s $^{-1}$, Araya et al. 2008) and it has a different V_{LSR} than expected (75.3 km s $^{-1}$ versus 73.6 km s $^{-1}$, Araya et al. 2008), thus, the emission feature they report could be an artifact caused by overlapping absorption lines.

G23.71–0.20 (IRAS 18324–0820): is a high-mass star-forming region located at distance of 6.21 kpc (Sanna et al. 2014a). The maser is located towards an extended radio continuum source (White et al. 2005; Araya et al. 2006). No HMC has been detected in this region (Rosero et al. 2013). The 6 cm formaldehyde maser overlaps with absorption (Figure 3). We measure a peak flux density of 71(8) mJy at 79.5 km s $^{-1}$, which is similar to the line parameters measured with the VLA in A configuration (Araya et al. 2006; 60 mJy beam $^{-1}$, 4.5 mJy beam $^{-1}$ rms, 79.2 km s $^{-1}$, Jan-

uary 2005) but greater than the VLA B-configuration measurement (Araya et al. 2006; 44 mJy beam⁻¹, 6 mJy beam⁻¹ rms, 79.2 km s⁻¹, April 2005). Although we cannot rule out low level variability, the formaldehyde maser in G23.71–0.20 did not show extreme variability between 2005 and 2009.

G25.83–0.18 (IRAS 18324–0820): is a massive star-forming region at a distance of 5 kpc (Green & McClure-Griffiths 2011) where formaldehyde masers were detected at the center of an infrared dark cloud (Araya et al. 2008). The source is characterized by 6.7 GHz masers and a HMC (Purcell et al. 2006). As reported by Araya et al. (2008), the maser is found at the blue-shifted wing of a formaldehyde absorption feature (Figure 3). We were able to simultaneously fit the main maser feature and the absorption (Figure 3). As in the case of NGC 7538 IRS 1 and IRAS 18566+0408, the formaldehyde maser in G25.83–0.18 has a double peak profile (Araya et al. 2008). In our spectrum, the weak formaldehyde maser component is significantly blended with the absorption and its line parameters cannot be measured. In the case of the main formaldehyde maser peak, no significant variability was detected with respect to the Araya et al. (2008) observations of 2005. No significant variability is seen with respect to the Chen et al. (2017) observations either.

G29.96–0.02 (IRAS 18434–0242): is a well known ultra-compact cometary HII region and HMC at a distance of 5.3 kpc (Reid et al. 2014). The HMC is located $\approx 2.6''$ to the West of the UCHII region, and the velocity structure of the HMC is consistent with a rotating massive toroid (Beltrán et al. 2011, Beltrán et al. 2013) with internal substructure (Beuther et al. 2007). The formaldehyde maser overlaps with absorption (Figure 3). We measured a maser peak flux density of 120(20) mJy at 100.4 km s⁻¹, which is twice the value observed by Hoffman et al. (2003), Pratap et al. (1994), and Chen et al. (2017). Future interferometric observations are needed to investigate variability of this maser.

IRAS 18566+0408 (G37.55+0.20): is the only known region where periodic flares of formaldehyde masers have been detected. The flares are correlated with 6.7 GHz methanol maser flares (Araya et al. 2010) and 6.035 GHz OH flares (Al-Marzouk et al. 2012; Halbe et al. 2016). IRAS 18566+0408 is located at a kinematic distance of 6.7 kpc (Araya et al. 2004b) and has bolometric luminosity about $6 \times 10^4 L_{\odot}$ (Zhang et al. 2007). We detected the formaldehyde maser in May 2008 and July 2009. As shown in Figure 3, no flares or significant variability of the maser were detected. The average (two epochs) of the peak flux density is 15 mJy at 79.4(0.2) km s⁻¹. Chen et al. (2017) also report detection of the maser, however, the line they found is significantly broader than previous observations (2.98 km s⁻¹ compared to < 2 km s⁻¹, e.g., Araya et al. 2007c). Further observations are needed to confirm changes in linewidth.

4.1.3. H₂¹³CO Absorption

As mentioned in Section 2, Figure 4 shows the H₂¹³CO absorption (blue) scaled up by a multiplicative factor to facilitate comparison with the main isotopologue line (6 cm H₂CO). In the case of NGC 7538 (Figure 4, bottom right panel), the H₂¹³CO absorption matches the main formaldehyde velocity component at -56 km s⁻¹, and we also find evidence for H₂¹³CO absorption at the velocity of the weaker formaldehyde line at -50 km s⁻¹. However, the weaker H₂¹³CO absorption at -50 km s⁻¹ is in part due to the hyperfine structure of the main absorption at -56 km s⁻¹. Following Wilson et al. (1976) and Henkel et al. (1980), we estimate a column density ratio $[H_2^{12}CO]/[H_2^{13}CO] = 30 \pm 20$ for the lower 6 cm K-doublet energy level⁶. This estimate takes into account the hyperfine structure of the H₂¹³CO line (Tucker et al. 1971, Wilson et al. 1976), and assumes $T_{ex} \sim T_{CMB}$, which implies optically thin absorption (note that Hoffman et al. (2003) reported optically thin 6 cm H₂CO absorption based on VLA CnB observations, i.e., $\tau = 0.093$). The large uncertainty in our $[H_2^{12}CO]/[H_2^{13}CO]$ determination is due to the low signal-to-noise of the H₂¹³CO detection (Figure 4), the uncertain values of excitation temperature and the photon trapping correction ($f_{12/13}$). We assume that the value of $f_{12/13}$ is between 1.0 and 1.4 (see Figure 4 of Henkel et al. 1980; optically thin absorption), given that the 6 cm H₂CO transition is likely to trace molecular gas with densities of less than $10^{5.5}$ cm⁻³ as observed in other star forming regions (e.g., Ginsburg et al. 2011 and Ginsburg et al. 2015). We note that based on H₂CO observations of the 29 GHz and 48 GHz transitions, McCauley et al. (2011) report greater molecular densities ($n(H_2) = 10^{5.78}$ cm⁻³), however the 6 cm H₂CO transition likely traces a larger fraction of the lower density molecular envelope. If the molecular density traced by the 6 cm H₂CO is greater than $10^{5.5}$ cm⁻³ and/or if the optical depth is greater (e.g., due to clumpiness or greater excitation temperature), then our $[H_2^{12}CO]/[H_2^{13}CO]$ determination would be a lower limit (e.g., Fomalont & Weliachew 1973; Whiteoak et al. 1974; Linke et al. 1977). Likewise, in the case of the other sources in our sample (Figure 4), the $[H_2^{12}CO]/[H_2^{13}CO]$ values have large uncertainties due to a combination of sensitivity, optical depth effects and unknown filling factors and excitation temperatures. Specifically, we obtain $[H_2^{12}CO]/[H_2^{13}CO]$

⁶ Hereafter, the $[H_2^{12}CO]/[H_2^{13}CO]$ refers to the column density ratio of the lower energy K-doublet of the 6 cm transition of both isotopologues.

$= 49 \pm 33$ (G29.96–0.02), > 30 (G23.01–0.41), > 60 (IRAS 18566+0408), and > 40 (G25.83–0.18). These values are similar to previous studies; for example, [Henkel et al. \(1985\)](#) reported H_2CO observations conducted with the 100 m Effelsberg Telescope toward six sources, including G29.9–0.0, which is a pointing position near G29.96–0.02 ($\sim 2.5'$ offset). They report a $[\text{H}_2^{12}\text{CO}]/[\text{H}_2^{13}\text{CO}]$ ratio of 45 ± 5 , which is very similar to the value we obtained for G29.96–0.02.

The $[\text{H}_2^{12}\text{CO}]/[\text{H}_2^{13}\text{CO}]$ value corresponds to the $^{12}\text{C}/^{13}\text{C}$ isotope ratio if no chemical differentiation between atomic $^{12}\text{C}/^{13}\text{C}$ and formaldehyde $[\text{H}_2\text{CO}]/[\text{H}_2^{13}\text{CO}]$ abundances occurs⁷. However, a number of studies have reported that ^{13}C abundance can be significantly lower in formaldehyde with respect to CO, which could be due to different chemical production paths of formaldehyde ([Watson et al. 1976](#); [Kutner et al. 1982](#); [Langer et al. 1984](#); [Wirström et al. 2012](#)). Keeping in mind the large uncertainty, the isotopic ratio we estimate in NGC 7538 is similar to the values obtained for sources in the Galactic Center (e.g., [Langer & Penzias 1990](#); [Giannetti et al. 2014](#)), even though NGC 7538 is located at a galactocentric distance of 9.8 kpc (derived from [Moscadelli et al. 2009](#)). If confirmed, this result would show that enhancements in H^{13}CO can be found far from the Galactic Center⁸. Interferometric mapping and higher signal-to-noise observations of both isotopologues and radio continuum (with matching (u, v) coverage) are necessary to reduce the uncertainties of the $[\text{H}_2^{12}\text{CO}]/[\text{H}_2^{13}\text{CO}]$ determinations for NGC 7538 and the other sources in our sample.

4.2. Methanol

4.2.1. 12.2 GHz CH_3OH Masers in NGC 7538 IRS 1

The 12.2 GHz methanol masers in NGC 7538 IRS 1 were first detected in 1985 by [Batra et al. \(1987\)](#) and re-observed in 1987 by [Koo et al. \(1988\)](#). The maser was characterized by a main velocity component at -56.5 km s^{-1} and weaker components at a velocity of $\sim -61.2 \text{ km s}^{-1}$. Long-term monitoring observations of the 12.2 GHz methanol masers in NGC 7538 IRS 1 were presented by [Pestalozzi et al. \(2012\)](#). They reported a linear decrease in flux density of the main velocity component (-56.5 km s^{-1}) during a period of almost two decades (6 VLBA observing epochs between 1995 and 2005, and the earlier data from [Batra et al. \(1987\)](#) and [Koo et al. \(1988\)](#)). The variability is characterized by a slope of $\sim -5.4 \text{ Jy year}^{-1}$. Our observations suggest that this trend has continued (at least until May 2010, Table 6), in particular, the flux density decrease between our 2008 and 2010 observations is $-3 \pm 2 \text{ Jy year}^{-1}$ (error obtained by assuming a 5% flux density calibration error, see section 2.1.2), and the extrapolation of the [Pestalozzi et al. \(2012\)](#) linear decrease matches our observations within 7%. [Pestalozzi et al. \(2012\)](#) mentioned that the variability trend of the main 12.2 GHz methanol component and possible spatial and spectral narrowing of the maser feature suggest saturated emission. We note that the velocity of the main 12.2 GHz methanol velocity component is similar to the velocity of the 6 cm H_2CO Component I (i.e., -56 km s^{-1} and -57.8 km s^{-1} , respectively), however, the masers are not spatially coincident (the main 12.2 GHz methanol maser is located at the 6.7 GHz methanol region A, Figure 1; see also Figure 2 of [Minier et al. 2002](#)).

[Menten \(1991\)](#) detected the 6.7 GHz methanol line in NGC 7538 IRS 1, which differed from the line profile of the 12.2 GHz line. Specifically, a 6.7 GHz methanol maser component at $\sim -58 \text{ km s}^{-1}$ was not present in the 12.2 GHz methanol spectra of [Batra et al. \(1987\)](#) and [Koo et al. \(1988\)](#). The absence of the $\sim -58 \text{ km s}^{-1}$ velocity component in the 12.2 GHz methanol spectra is also seen in Figure 1 of [Minier et al. \(2000\)](#) based on VLBA observations conducted between 1997 and 1999. As shown in our spectra (Figure 5), several 12.2 GHz methanol maser features are present at $\sim -58 \text{ km s}^{-1}$ in our 2008 and 2010 data, with flux densities of the order of 10 Jy. [Moscadelli et al. \(2009\)](#) also reported 12.2 GHz methanol masers at $\sim -58 \text{ km s}^{-1}$ based on VLBA observations conducted in 2005 and 2006, but they reported smaller flux densities (0.1 Jy). The flux density difference between our 2008 and 2010 observations and [Moscadelli et al. \(2009\)](#) values could be caused by spatial-filtering of 12.2 GHz signal by the VLBA in addition to intrinsic maser variability. In contrast to the early 12.2 and 6.7 GHz methanol detections, all velocity components in our 2008 and 2010 12.2 GHz methanol spectra (Figure 5) have corresponding features in more recent 6.7 GHz methanol spectra, e.g., the spectra obtained with MERLIN in 2005 and EVN in 2009 ([Surcis et al. 2011](#)). Thus, with the appearance of the -58 km s^{-1} features, the 12.2 GHz methanol maser profile in NGC 7538 IRS 1 has changed from showing clear differences with respect to the 6.7 GHz profile, to becoming remarkably similar within two decades. According to the statistical study of [Breen et al. \(2011\)](#), sources with both 6.7 and 12.2 GHz methanol masers may be more evolved than regions with only 6.7 GHz masers. Follow up observations of the 12.2 GHz methanol masers in

⁷ See [Wilson et al. \(1976\)](#) for assumptions in the determination of the $^{12}\text{C}/^{13}\text{C}$ isotope ratio based on H_2^{13}CO and H_2CO observations.

⁸ We note that [Feng et al. \(2016a\)](#) recently derived H_2CO column densities assuming a smaller H_2^{13}CO abundance in NGC 7538 S by using $^{12}\text{C}/^{13}\text{C} = 73$ ([Giannetti et al. 2014](#)).

the region are required to explore whether their emergence from 1986 to ~ 2005 is indicative of stochastic variability, which would cast doubts on the reliability of using 6.7 and 12.2 GHz methanol masers as evolutionary indicators.

4.2.2. Methanol Absorption

We detected two K-Band methanol transitions: 20.9706510 GHz (torsionally excited, $E_{up} = 452$ K) and 20.1710890 GHz (torsional ground state, $E_{up} = 166$ K) in three observing runs (epochs 1, 2, and 5; see Table 6 and Figure 5). The line parameters are similar to those reported by Menten et al. (1986), and the apparent variability of the line parameters seen in our data is likely caused by calibration and pointing variations in addition to the large rms (Figure 5). We also report detection of weak absorption (-12 mJy at -60 km s $^{-1}$; rms = 3 mJy) of the 14.782212 GHz $^{13}\text{CH}_3\text{OH}$ isotopologue toward NGC 7538 IRS 1. We detected the weak line in two epochs (epochs 1 and 5, see Figure 5). This transition corresponds to the 12.2 GHz line of the main methanol isotopologue, thus, it is very likely that the 12.2 GHz methanol line also has absorption in NGC 7538 IRS 1, but the absorption is blended with the strong 12.2 GHz methanol masers and thus could not be detected.

We note that additional thermal methanol transitions have been recently observed towards NGC 7538 IRS 1 in the millimeter range (Beuther et al. 2013; Feng et al. 2016b). Interestingly, while some of the lower excited transitions were seen in absorption, several other transitions showed emission lines (see Feng et al. 2016b, their Table 5). No clear trend for absorption or emission could be seen with regard to A- or E-symmetry, or regarding torsionally excited vs. ground state. But it appeared that transitions with upper-level energies >250 K usually show emission. This tentative trend is not obeyed in our data where the 20.97 GHz transition appears in absorption despite its high upper-level energy of 452 K. One has to keep in mind, however, that our observations were conducted with a single dish telescope (GBT) while Feng et al. (2016b) report Plateau de Bure Interferometre data, and that the underlying continuum is dominated in our case by free-free emission, while for the observations listed in Feng et al. (2016b), the continuum is a mixture of free-free emission with a steeply rising contribution from thermal dust. The small-scale brightness temperature distribution in the continuum is different between the two regimes.

4.3. Water Masers

Our three epoch spectra of the water masers in NGC 7538 IRS 1 (2008, 2009, and 2010; Figure 6) exemplifies the well-known characteristic of high level of variability of water masers (e.g., Colom et al. 2015, Lekht et al. 2007, Liljestrom et al. 1989). In contrast to many of the weak components that appeared/disappeared during our observations, the brightest maser component at -58.2 km s $^{-1}$ was detected in all three epochs, and showed a decrease rate in the flux density of -20 ± 6 Jy year $^{-1}$. The maser was also observed by Hoffman & Kim (2011) with the GBT in three epochs (2010 November 24; 2010 December 8; and 2011 January 22)⁹. The decreasing trend of the main peak of the water maser continued to at least 2011, i.e., including the Hoffman & Kim (2011) data with ours, the slope of the variability trend is -33 ± 6 Jy year $^{-1}$. This variability slope is steeper than the one of the 12.2 GHz methanol maser (-3 ± 2 Jy year $^{-1}$, see Sect. 4.2.1).

As in the case of the main 12.2 GHz methanol maser velocity component, the main component of the 22.2 GHz water masers has approximately the same peak velocity (-58.2 km s $^{-1}$) as Component I of the 6 cm formaldehyde maser (-57.8 km s $^{-1}$), both show a negative flux density rate of change, and the masers are not spatially coincident at sub-arcsecond resolution (e.g., see Surcis et al. 2011 and Galván-Madrid et al. 2010). However, in contrast to the formaldehyde masers, significant radial velocity drift of the water maser components is observed over the years, which makes it difficult to track the evolution of individual maser components, particularly when comparing results from different telescopes and different epochs. A thorough discussion of the water maser variability and contamination of the spectra due to emission in the GBT side lobe is presented in Hoffman & Kim (2011) (see also Lekht & Munitsyn 2010 and references therein).

5. SUMMARY

We present results of observations of the 6 cm formaldehyde masers towards NGC 7538 IRS 1 conducted in nine epochs (2008 - 2015) with the GBT, WRST, and VLA. The main goal of the observations was to further investigate the possibility of similar variability between the two maser velocity components as proposed by Araya et al. (2007b).

⁹ The velocities of the H₂O maser lines listed in Hoffman & Kim (2011) differ from ours by ~ 0.6 km s $^{-1}$ because of different assumed rest frequencies; instead of the frequency used in this work [22.23508 GHz, Splatalogue], Hoffman & Kim (2011) used the 6(1,6)-5(2,3) F=5-4 frequency of 22.2351204 GHz (LOVAS database).

Our data show that the similar variability behavior has continued (with a time shift of ~ 15 years). The similar variability may indicate that the two maser regions have similar physical dimensions and morphologies and that the maser variability could be explained by a slow change in the line-of-sight maser amplification path, perhaps related to the kinematics of the maser clouds (e.g., rotation of non-spherical maser clouds). In addition, 6 cm formaldehyde masers were observed toward five other star forming regions. Four of them (G23.01–0.20, G23.71–0.20, G25.83–0.18, and IRAS 18566+0408) showed no flux density variability (IRAS 18566+0408 was observed during the quiescent phase of the maser). In G29.96–0.02, we detect a possible increase in flux density, however the line is blended with strong absorption, thus, interferometric observations are needed to confirm variability of this maser.

We also report observations of the H_2^{13}CO isotopologue of the 6 cm H_2CO transition toward the six 6 cm H_2CO maser regions in our sample. No emission was detected, but weak H_2^{13}CO absorption lines were found in all sources except G23.71–0.20. Due to low sensitivity and uncertainties in filling factors and excitation temperatures, a high precision determination of the $^{12}\text{C}/^{13}\text{C}$ isotope ratio could not be obtained. However, the NGC 7538 data are consistent with a low ratio, similar to Galactic Center values. Higher signal-to-noise observations are needed to confirm this possibility.

The spectra of other masers (22.2 GHz water and 12.2 GHz methanol masers) were also observed toward NGC 7538 IRS 1. We found that the strongest maser components of 22.2 GHz water and 12.2 GHz methanol masers steadily decreased in flux density during our observations. In the case of the 22.2 GHz water masers, the flux density variability of the main velocity component (-58.2 km s^{-1}) is consistent with GBT observations of water masers in this region observed between 2010 and 2011 by Hoffman & Kim (2011). We point out that the velocity of the main water maser peak is similar to the velocity of the 6 cm formaldehyde maser Component I and both showed a negative flux density rate of change. In the case of the methanol masers, Pestalozzi et al. (2012) reported that the flux density of the main 12.2 GHz maser component (approximately at -56.0 km s^{-1}) decreased at a rate of about 5.4 Jy year^{-1} between 1995 and 2005. Our two measurements of the 12.2 GHz masers show that such monotonic variability continued until at least May 2010.

Previous observations of the 12.2 GHz methanol masers towards NGC 7538 IRS 1 over the last two decades showed that some velocity components were not present at the velocities of some of the 6.7 GHz maser peaks, and thus, the spectral line profiles of 12.2 and 6.7 GHz masers were different. Our data now show that these missing 12.2 GHz velocity components appeared and increased in flux density, and the overall spectral profiles of both transitions are now very similar. We also detected two other methanol transitions in absorption at 20.17 and 20.97 GHz, and weak absorption of $^{13}\text{CH}_3\text{OH}$ at 14.8 GHz, which corresponds to the 12.2 GHz transition of the main isotopologue. Therefore, it is very likely that the main isotopologue also shows absorption, but it was not detected because of spectral blending with strong 12.2 GHz methanol masers.

We thank the anonymous referee for constructive comments that helped us improve the manuscript. The National Radio Astronomy Observatory is a facility of the National Science Foundation operated under cooperative agreement by Associated Universities, Inc. I.M.H. thanks the WSRT staff for flexible scheduling of the array and thanks S. R. DeSoto for assistance in data reduction. P.H. acknowledges partial support from NSF grant AST-0908901. This work has made use of the computational facilities donated by Frank Rodeffer to the Astrophysics Research Laboratory of Western Illinois University. We also acknowledge a former WIU student, Edita Ezerskyte, for participation in early stages of this project. This research made use of the NASA’s Astrophysics Data System and SIMBAD.

Software: GBTIDL, AIPS (van Moorsel et al. 1996), CASA (McMullin et al. 2007), CLEO.

REFERENCES

- Al-Marzouk, A. A., Araya, E. D., Hofner, P., et al. 2012, *ApJ*, 750, 170
- Araya, E., Baan, W. A., & Hofner, P. 2004a, *ApJS*, 154, 541
- Araya, E., Hofner, P., & Goss, W. M. 2007a, in *IAU Symp.* 242, *Astrophysical Masers and their Environments*, ed. J. M. Chapman & W. A. Baan (Cambridge: Cambridge Univ. Press), 110
- Araya, E., Hofner, P., Goss, W. M., et al. 2006, *ApJL*, 643, L33
- Araya, E., Hofner, P., Goss, W. M., et al. 2007b, *ApJS*, 170, 152
- Araya, E. D., Hofner, P., Goss, W. M., et al. 2008, *ApJS*, 178, 330-338
- Araya, E. D., Hofner, P., Goss, W. M., et al. 2010, *ApJL*, 717, L133
- Araya, E., Hofner, P., Linz, H., et al. 2004b, *ApJS*, 154, 579
- Araya, E., Hofner, P., Sewilo, M., et al. 2007c, *ApJL*, 654, L95
- Araya, E. D., Olmi, L., Morales Ortiz, J., et al. 2015, *ApJS*, 221, 10
- Baan, W. A. 1985, *Nature*, 315, 26
- Baan, W. A., Guesten, R., & Haschick, A. D. 1986, *ApJ*, 305, 830
- Bartkiewicz, A., Szymczak, M., van Langevelde, H. J., Richards, A. M. S., & Pihlström, Y. M. 2009, *A&A*, 502, 155
- Batrla, W., Matthews, H. E., Menten, K. M., & Walmsley, C. M. 1987, *Nature*, 326, 49
- Beltrán, M. T., Cesaroni, R., Neri, R., & Codella, C. 2011, *A&A*, 525, A151
- Beltrán, M. T., Olmi, L., Cesaroni, R., et al. 2013, *A&A*, 552, A123
- Beuther, H., Linz, H., Henning, Th. 2013, *A&A*, 558, A81
- Beuther, H., Linz, H., Henning, T., Feng, S., & Teague, R. 2017, *arXiv:1705.06246*
- Beuther, H., Zhang, Q., Bergin, E. A., et al. 2007, *A&A*, 468, 1045
- Biraud, F., Bourgois, G., Crovisier, J., et al. 1974, *A&A*, 34, 163
- Bockelee-Morvan, D., Crovisier, J., Colom, P., & Despois, D. 1994, *A&A*, 287, 647
- Breen, S. L., Ellingsen, S. P., Caswell, J. L., et al. 2011, *ApJ*, 733, 80
- Breen, S. L., Ellingsen, S. P., Contreras, Y., et al. 2013, *MNRAS*, 435, 524
- Brunthaler, A., Reid, M. J., Menten, K. M., et al. 2009, *ApJ*, 693, 424
- Chen, X., Shen, Z.-Q., Li, X.-Q., et al. 2017, *MNRAS*, 466, 4364
- Colom, P., Lekht, E. E., Pashchenko, M. I., & Rudnitskij, G. M. 2015, *A&A*, 575, A49
- Cyganowski, C. J., Brogan, C. L., Hunter, T. R., & Churchwell, E. 2009, *ApJ*, 702, 1615
- Downes, D., & Wilson, T. L. 1974, *ApJL*, 191, L77 b
- Downes, D., Wilson, T. L., Bieging, J., & Wink, J. 1980, *A&AS*, 40, 379
- Felli, M., Brand, J., Cesaroni, R., et al. 2007, *A&A*, 476, 373
- Feng, S., Beuther, H., Semenov, D., et al. 2016a, *A&A*, 593, A4
- Feng, S., Beuther, H., Zhang, Q., et al. 2016b, *A&A*, 592, A21
- Fomalont, E. B., & Weliachew, L. 1973, *ApJ*, 181, 781
- Frail, D. A., Goss, W. M., & Slysh, V. I. 1994, *ApJL*, 424, L111
- Furuya, R. S., Cesaroni, R., Takahashi, S., et al. 2008, *ApJ*, 673, 363
- Galván-Madrid, R., Montes, G., Ramírez, E. A., et al. 2010, *ApJ*, 713, 423
- Gaume, R. A., Goss, W. M., Dickel, H. R., Wilson, T. L., & Johnston, K. J. 1995, *ApJ*, 438, 776
- Giannetti, A., Wyrowski, F., Brand, J., et al. 2014, *A&A*, 570, A65
- Ginsburg, A., Darling, J., Battersby, C., Zeiger, B., & Bally, J. 2011, *ApJ*, 736, 149
- Ginsburg, A., Bally, J., Battersby, C., et al. 2015, *A&A*, 573, A106
- Goddi, C., Moscadelli, L., & Sanna, A. 2011, *A&A*, 535, L8
- Goddi, C., Zhang, Q., & Moscadelli, L. 2015, *A&A*, 573, A108
- Goedhart, S., Gaylard, M. J., & van der Walt, D. J. 2003, *MNRAS*, 339, L33
- Goedhart, S., Gaylard, M. J., & van der Walt, D. J. 2004, *MNRAS*, 355, 553
- Goedhart, S., Gaylard, M. J., & van der Walt, D. J. 2012, in *IAU Symp.* 287, *Cosmic Masers - from OH to H0*, ed. R. S. Booth, E. M. L. Humphreys & W. H. T. Vlemmings (Cambridge: Cambridge Univ. Press), 85
- Goedhart, S., Maswanganye, J. P., Gaylard, M. J., & van der Walt, D. J. 2014, *MNRAS*, 437, 1808
- Green, J. A., & McClure-Griffiths, N. M. 2011, *MNRAS*, 417, 2500
- Halbe, D. M., Araya, E., Hofner, P., et al. 2016, *American Astronomical Society Meeting Abstracts*, 227, 347.02
- Haschick, A. D., Baan, W. A., & Peng, E. W. 1994, *ApJL*, 437, L35
- Henkel, C., Guesten, R., & Gardner, F. F. 1985, *A&A*, 143, 148

- Henkel, C., Walmsley, C. M., & Wilson, T. L. 1980, *A&A*, 82, 41
- Henkel, C., Wilson, T. L., & Bieging, J. 1982, *A&A*, 109, 344
- Hoffman, I. M., Goss, W. M., & Palmer, P. 2007, *ApJ*, 654, 971
- Hoffman, I. M., Goss, W. M., Palmer, P., & Richards, A. M. S. 2003, *ApJ*, 598, 1061
- Hoffman, I. M., & Kim, S. S. 2011, *AJ*, 142, 202
- Keto, E., Zhang, Q., & Kurtz, S. 2008, *ApJ*, 672, 423-432
- Koo, B.-C., Williams, D. R. D., Heiles, C., & Backer, D. C. 1988, *ApJ*, 326, 931
- Kutner, M. L., Machnik, D. E., Tucker, K. D., & Massano, W. 1982, *ApJ*, 254, 538
- Langer, W. D., Graedel, T. E., Frerking, M. A., & Armentrout, P. B. 1984, *ApJ*, 277, 581
- Langer, W. D., & Penzias, A. A. 1990, *ApJ*, 357, 477
- Lekht, E. E., & Munitsyn, V. A. 2010, *Astronomy Reports*, 54, 151
- Lekht, E. E., Munitsyn, V. A., & Krasnov, V. V. 2007, *Astronomy Reports*, 51, 27
- Liljestrom, T., Mattila, K., Toriseva, M., & Anttila, R. 1989, *A&AS*, 79, 19
- Linke, R. A., Goldsmith, P. F., Wannier, P. G., Wilson, R. W., & Penzias, A. A. 1977, *ApJ*, 214, 50
- Lo, K. Y. 2005, *ARA&A*, 43, 625
- Luisi, M., Anderson, L. D., Balser, D. S., Bania, T. M., & Wenger, T. V. 2016, *ApJ*, 824, 125
- Mangum, J. G., Darling, J., Menten, K. M., & Henkel, C. 2008, *ApJ*, 673, 832-846
- Maswanganye, J. P., van der Walt, D. J., Goedhart, S., & Gaylard, M. J. 2016, *MNRAS*, 456, 4335
- McCauley, P. I., Mangum, J. G., & Wootten, A. 2011, *ApJ*, 742, 58
- McMullin, J. P., Waters, B., Schiebel, D., Young, W., & Golap, K. 2007, *Astronomical Data Analysis Software and Systems XVI*, 376, 127
- Mehringer, D. M., Goss, W. M., & Palmer, P. 1994, *ApJ*, 434, 237
- Menten, K. M. 1991, *ApJL*, 380, L75
- Menten, K. M., Walmsley, C. M., Henkel, C., et al. 1986, *A&A*, 169, 271
- Minier, V., Booth, R. S., & Conway, J. E. 2000, *A&A*, 362, 1093
- Minier, V., Booth, R. S., & Conway, J. E. 2002, *A&A*, 383, 614
- Moscadelli, L., & Goddi, C. 2014, *A&A*, 566, A150
- Moscadelli, L., Reid, M. J., Menten, K. M., et al. 2009, *ApJ*, 693, 406
- Moscadelli, L., Sanna, A., & Goddi, C. 2011, *A&A*, 536, A38
- Müller, H. S. P., Schlöder, F., Stutzki, J., & Winnewisser, G. 2005, *Journal of Molecular Structure*, 742, 215
- Perley, R. A., & Butler, B. J. 2013, *ApJS*, 204, 19
- Pestalozzi, M., Jerkstrand, A., & Conway, J. 2012, *Cosmic Masers - from OH to H0*, 287, 186
- Pickett, H. M., Poynter, R. L., Cohen, E. A., et al. 1998, *JQSRT*, 60, 883
- Pogrebenko, S. V., Gurvits, L. I., Elitzur, M., et al. 2009, *A&A*, 494, L1
- Pratap, P., Menten, K. M., & Snyder, L. E. 1994, *ApJL*, 430, L129
- Purcell, C. R., Balasubramanyam, R., Burton, M. G., et al. 2006, *MNRAS*, 367, 553
- Reid, M. J., Menten, K. M., Brunthaler, A., et al. 2014, *ApJ*, 783, 130
- Robinson, B. J., & McGee, R. X. 1967, *ARA&A*, 5, 183
- Rosero, V., Hofner, P., Kurtz, S., Bieging, J., & Araya, E. D. 2013, *ApJS*, 207, 12
- Rots, A. H., Dickel, H. R., Forster, J. R., & Goss, W. M. 1981, *ApJL*, 245, L15
- Sanna, A., Moscadelli, L., Cesaroni, R., et al. 2010, *A&A*, 517, A78
- Sanna, A., Reid, M. J., Menten, K. M., et al. 2014a, *ApJ*, 781, 108
- Sanna, A., Cesaroni, R., Moscadelli, L., et al. 2014b, *A&A*, 565, A34
- Sewilo, M., Churchwell, E., Kurtz, S., Goss, W. M., & Hofner, P. 2004a, *ApJ*, 605, 285
- Sjouwerman, L. O., Murray, C. E., Pihlström, Y. M., Fish, V. L., & Araya, E. D. 2010, *ApJL*, 724, L158
- Surcis, G., Vlemmings, W. H. T., Torres, R. M., van Langevelde, H. J., & Hutawarakorn Kramer, B. 2011, *A&A*, 533, A47
- Szymczak, M., Olech, M., Wolak, P., Bartkiewicz, A., & Gawroński, M. 2016, *MNRAS*, 459, L56
- Torrelles, J. M., Patel, N. A., Curiel, S., et al. 2011, *MNRAS*, 410, 627
- Tucker, K. D., Tomasevich, G. R., & Thaddeus, P. 1971, *ApJ*, 169, 429
- Turner, B. E. 1974, *ApJL*, 189, L137
- van Moorsel, G., Kembell, A., & Greisen, E. 1996, *Astronomical Data Analysis Software and Systems V*, 101, 37
- Walsh, A. J., Burton, M. G., Hyland, A. R., & Robinson, G. 1998, *MNRAS*, 301, 640
- Watson, W. D., Anicich, V. G., & Huntress, W. T., Jr. 1976, *ApJL*, 205, L165

- Weaver, H., Williams, D. R. W., Dieter, N. H., & Lum, W. T. 1965, *Nature*, 208, 29
- White, R. L., Becker, R. H., & Helfand, D. J. 2005, *AJ*, 130, 586
- Whiteoak, J. B., & Gardner, F. F. 1983, *MNRAS*, 205, 27
- Whiteoak, J. B., Rogstad, D. H., & Lockhart, I. A. 1974, *A&A*, 36, 245
- Wilson, W. J., & Barrett, A. H. 1968, *Science*, 161, 778
- Wilson, T. L., Bieging, J., Downes, D., & Gardner, F. F. 1976, *A&A*, 51, 303
- Wiström, E. S., Charnley, S. B., Geppert, W. D., & Persson, C. M. 2012, *Lunar and Planetary Science Conference*, 43, 1611
- Wood, D. O. S., & Churchwell, E. 1989, *ApJS*, 69, 831
- Zhang, Q., Sridharan, T. K., Hunter, T. R., et al. 2007, *A&A*, 470, 269